NUREG/CR-3504
EPRI NP-3546
ANL-83-65

NUREG/CR-3504
EPRI NP-3546
ANL-83-65

TURBULENCE MODELING IN THE COMMIX COMPUTER CODE

by

F. F. Chen, H. M. Domanus,
W. T. Sha, and V. L. Shah

ARGONNE NATIONAL LABORATORY, ARGONNE, ILLINOIS
Operated by THE UNIVERSITY OF CHICAGO

Prepared for the Office of Nuclear Regulatory Research
U. S. NUCLEAR REGULATORY COMMISSION
under Interagency Agreement DOE 40-550-75

Argonne National Laboratory, with facilities in the states of Illinois and Idaho, is owned by the United States government, and operated by The University of Chicago under the provisions of a contract with the Department of Energy.

Available from

GPO Sales Program
Division of Technical Information and Document Control
U. S. Nuclear Regulatory Commission
Washington, D.C. 20555

and

National Technical Information Service
Springfield, Virginia 22161

NUREG/CR-3504
EPRI NP-3546
ANL-83-65

Distribution
Category: R7

ARGONNE NATIONAL LABORATORY
9700 South Cass Avenue
Argonne, Illinois 60439

TURBULENCE MODELING IN THE COMMIX COMPUTER CODE

by

F. F. Chen, H. M. Domanus, W. T. Sha, and V. L. Shah

Prepared by

Analytical Thermal Hydraulic Research Program
Components Technology Division

April 1984

Prepared for

Office of Nuclear Regulatory Research
U.S. Nuclear Regulatory Commission
Washington, D.C. 20555
under Interagency Agreement DOE 40-550-75

NRC FIN No. A2045

TURBULENCE MODELING IN THE COMMIX COMPUTER CODE

by

F. F. Chen, H. M. Domanus, W. T. Sha, and V. L. Shah

ABSTRACT

The report describes the three additional turbulence models [0-equation (mixing length), 1-equation (k), and 2-equation ($k-\epsilon$)] recently implemented in the COMMIX-1B computer code. COMMIX-1B is a three-dimensional, steady-state/transient, single-phase computer code for thermal-hydraulic analysis of single/multicomponent systems under normal and off-normal operating conditions. All three turbulence models are provided as options, and a user can select the one that is most appropriate for his or her application.

To validate these turbulence models, we have performed several numerical simulations and compared the results with experimental data. Three of the simulations--turbulent flow in a pipe, flow in a circular duct with sudden expansion, and thermal and fluid mixing in the cold leg and downcomer of a PWR--are presented here along with their comparisons with experimental data. More analyses are needed for further validation. Incorporation of the three turbulence models has expanded the range of application of the COMMIX code.

FIN No.	Title
A2045	3-D Time-Dependent Code Development

CONTENTS

CONTENTS (Contd.)

LIST OF FIGURES

TABLES

EXECUTIVE SUMMARY

COMMIX-1 computer code has been developed for three-dimensional, steady-state/transient single-phase thermal hydraulic analysis of a single-component/multicomponent system under normal/off-normal operating conditions. In the initial development of COMMIX-1 and COMMIX-1A (advanced version) we had implemented a simple constant turbulent viscosity model to account for the turbulence. To expand the range of COMMIX applicability, we have implemented three additional turbulence models in COMMIX-1B (the extended version of COMMIX-1A). They are:

Zero-equation mixing-length model,

One-equation (k) model, and

Two-equation ($k-\varepsilon$) model.

Furthermore, in the two-equation ($k-\varepsilon$) model, we have provided two possible options: (i) high-Reynolds number flow model and (ii) low-Reynolds number flow model. In the case of high-Reynolds number flow model, we use a special wall-function treatment to account for large variations in the values of turbulence quantities in the vicinity of a solid wall. Whereas, in the case of low-Reynolds number flow model, a special wall-function treatment is not required because we include the laminar diffusive transport terms in the conservation equations.

The present report describes, after a brief background on turbulence modeling, the governing equations and formulations of the three turbulence models. We have also presented the results of three numerical simulations performed for the validation The problems simulated are:

- Turbulent flow in a pipe,
- Flow in a circular duct with sudden expansion,
- Thermal and fluid mixing in the cold leg and downcomer of a pressurized water reactor.

These validation efforts were motivated by the need to implement a better turbulence model in the COMMIX codes for the analysis of thermal mixing. Accurate predictions of thermal mixing is important in resolving the so-called pressurized thermal shock issue, which has been an urgent safety issue in the nuclear industry[22,23,25].

It may be concluded that the implementation of three additional turbulence models has augmented the applicability of COMMIX code. We can now perform analysis of recirculating, highly buoyant, and thermally stratified turbulent flows with COMMIX.

1. INTRODUCTION

COMMIX-1B, the extended version of COMMIX-1A, is a three-dimensional, steady-state/transient, single-phase computer code for thermal-hydraulic analysis of reactor component/multicomponent systems under normal and off-normal operating conditions. The code employs a new porous-media formulation[1,2] to model geometrical and physical effects due to the presence of stationary structures in a flow domain. The concepts of volume porosity and directional surface permeability account for geometrical effects. Volume porosity is defined as the ratio of volume occupied by fluid in a control volume to the total control volume; directional surface permeability is defined as the fraction of the control surface in a given direction through which the fluid flows freely.

In the development of COMMIX-1[3] and COMMIX-1A[4], we implemented, for simplicity, a constant turbulent viscosity model to account for the turbulence in a flow domain. We found that in many cases, a simple constant turbulent viscosity model along with proper correlations for distributed resistance and heat transfer coefficient is adequate to predict essential thermal-hydraulic characteristics. However, in other cases, this simplified approach of turbulence modeling is inadequate.

Recently, we were engaged in determining the thermal mixing in a PWR cold leg and downcomer with a high-pressure injection system that is associated with the so-called pressurized thermal shock issue[22-25]. During the analysis, we observed that for moderately high Reynolds numbers and low Froude number, the interaction of buoyancy and turbulence plays a very important role in characterizing thermal stratification. A simple constant turbulent viscosity model is not adequate to predict the essential thermal-hydraulic behavior in such highly buoyant, turbulent flows.

Therefore, three additional turbulence models have been implemented in COMMIX:

Zero-equation mixing-length model,

One-equation (k) model, and

Two-equation (k-ε) model.

These are provided as additional options for users of COMMIX. These new turbulence-model options have extended the capability of COMMIX to predict system performance over a wide range of operating conditions.

To validate the new turbulence models, several numerical computations have been performed and the results were compared with experimental data. In this report, a brief description of these turbulence models is given and the results are presented for the following three numerical simulations:

Isothermal turbulent flow in a pipe,

Isothermal turbulent flow in a duct with abrupt expansion, and

Thermal and fluid mixing in the cold leg and downcomer of a pressurized water reactor.

We can see from the comparisons that the turbulence models implemented in COMMIX, are capable of analyzing recirculating, highly buoyant, and thermally stratified turbulent flows reasonably well.

2. BACKGROUND ON TURBULENCE MODELING

The subject of turbulence has attracted countless researchers over a period of more than 80 years. In 1895, Reynolds proposed that a fluid particle in turbulent flow is in randomly unsteady motion. He averaged the Navier Stokes equation over a time-scale that is long compared with the turbulent time scale, and derived the equations that describe the mean turbulent motion. Why then has the problem of turbulence not been resolved completely? It is due to the following three major difficulties:

- The appearance of the time-averaged correlations, such as $\rho\overline{u_i u_j}$, in the governing equations, give rise to the so called "closure" problem. Here ρ denotes fluid density, u_i and u_j are the fluctuating velocity components in the coordinate directions x_i and x_j, respectively and the overbar denotes the time averaging. The correlations, $\rho\overline{u_i u_j}$, are known as "Reynolds Stresses". The Reynolds stresses are very important in any turbulent shear flows and are the source of analytic difficulties.

- The other difficulty is that the constituents of the turbulence phenomenon normally take place in scales of motion that are very small orders of magnitude in size while the whole flow domain may extend over meters or even kilometers. Important details of turbulence are small-scale in character (although it is not the details but the time-averaged consequences that are of interest in practical appplication). As a result, the computational nodes required to resolve small-scale motions of turbulence will far exceed the storage capacity of the current computers. The corresponding computer running time also will be unfeasibly long.

- An alternative to small scale turbulence details is to employ some form of turbulence modeling wherein we need to solve time-averaged equations of motion along with a set of transport equations of turbulence quantities, e.g. -- k- the turbulence kinetic energy, ε- the rate of dissipation of k, etc. It is only now with recent advances in computer power, that some turbulence modeling can be carried out.

Many turbulence models have been proposed to resolve these three difficulties by providing solvable equations for computation of turbulent flows. The most popular model, yet the simplest, is the mixing-length hypothesis generally attributed to Prandtl[5]. Here, we refer the mixing length hypothesis as a 0-equation model because it does not require solution of any additional equation.

In 1945, Prandtl[6] suggested a more general approach than the mixing-length hypothesis. His new approach is generally referred to as a one-equation turbulence model. In this model, the square root of the turbulence kinetic energy, k, is the characteristic fluctuating velocity. To determine the value of k, we need to solve its transport equation. Since then, many one-equation turbulence models have been proposed. The transport equation for the shear stress developed by Bradshaw et al.[7] and the transport equation for the turbulent viscosity developed by Nee and Kovasznay[8] are typical.

Undoubtedly, one-equation models generally produce more reliable results than the mixing-length hypothesis for most of the computations. However, a need to obtain a more accurate estimate of the length scale distribution, especially in the separated flow region, leads to the suggestion of two-equation turbulence models.

There are several two-equation turbulence models: k-ε, k-ℓ, k-W, etc. The symbol k is the kinetic energy of turbulence, ε is the dissipation rate of turbulence energy, ℓ is a macroscopic length scale of turbulence, and W is interpreted as the time-averaged square of the velocity fluctuations. Among the two-equation models, the k-ε model, proposed by Harlow and Nakayama[9] and Jones and Launder[10], is the most widely used.

The next level in turbulence modeling is represented by the complex Reynolds stress models[11-14]. These models are still in the development stage. We have therefore programmed in COMMIX only the 0-, 1-, and 2-equation turbulence models for the analysis of turbulent flows. These models are described in the following sections.

As we increase the level of turbulence modeling from 0- to 1-equation, from 1- to 2-equation, and so forth, we are adding more and more complexity to the computer programming. Computer cost increases with the increase in level of turbulence model. So during the selection of a turbulence model, we must balance the amount of desired increase in accuracy with the additional cost of computing.

3. GOVERNING EQUATIONS

The governing instantaneous Navier-Stokes equations for turbulent flow, in the Cartesian tensor notation, are

$$\frac{\partial \rho}{\partial t} + \frac{\partial}{\partial x_i}\left(\rho \hat{U}_i\right) = 0 \ , \tag{3.1}$$

$$\rho\left(\frac{\partial \hat{U}_i}{\partial t} + \hat{U}_j \frac{\partial \hat{U}_i}{\partial x_j}\right) = -\frac{\partial \hat{P}}{\partial x_i} + \frac{\partial}{\partial x_j}\hat{\tau}_{ji} + \hat{\rho} g_i \ , \tag{3.2}$$

and

$$\hat{\tau}_{ij} = \mu\left(\frac{\partial \hat{U}_i}{\partial x_j} + \frac{\partial \hat{U}_j}{\partial x_i}\right) - \frac{2}{3}\delta_{ij}\,\mu\,\frac{\partial \hat{U}_k}{\partial x_k} \ . \tag{3.3}$$

Here, $\hat{U}_i$ represents the instantaneous values of velocity, $\hat{P}$ is the instantaneous static pressure, ρ is the instantaneous density, x_i's are the Cartesian coordinates, g_i is the gravitational acceleration vector, μ is the molecular viscosity, and $\hat{\tau}_{ij}$ is the stress tensor. We note that the instantaneous density is retained only in the buoyancy term. Elsewhere, the mean density ρ is used.

In the derivation of the mean flow equations, it is assumed that we can specify all instantaneous values as a sum of their temporal mean value and a fluctuating component, e.g.,

$$\hat{U}_i = U_i + u_i \ . \tag{3.4}$$

Here, U_i is the mean flow velocity based on a time average, defined by

$$U_i = \lim_{T\to\infty} \frac{1}{T} \int_{t_o}^{t_o+T} \hat{U}_i \, dt \ . \tag{3.5}$$

The averaging time T is chosen such that it is long when compared to the turbulence time scale, but short when compared to the time needed for appreciable ordered variations to occur.

After applying Assumption 3.4 and time-averaging Eqs. 3.1 and 3.2 over the interval T, the equations of motion for mean flow are:

$$\frac{\partial \rho}{\partial t} + \frac{\partial \rho U_i}{\partial x_i} = 0 \ , \tag{3.6}$$

and

$$\rho \left(\frac{\partial U_i}{\partial t} + U_j \frac{\partial U_i}{\partial x_j} \right) = - \frac{\partial P}{\partial x_i} + \frac{\partial \tau_{ji}}{\partial x_j} - \frac{\partial \rho \overline{u_i u_j}}{\partial x_j} + \rho g_i \ . \tag{3.7}$$

Equation 3.7 is generally known as the Reynolds equation. The correlation terms, $\rho u_i u_j$, in Eq. 3.7 are called Reynolds stresses. They represent additional momentum fluxes or apparent stresses in the fluid over and above those associated with the mean motion. Because the fluctuating components in the Reynolds stresses are not a priori known, the momentum and continuity equations do not form a closed set[14,15].

4. APPROXIMATION OF REYNOLDS STRESSES

To make the turbulent flow a closure problem, many turbulence models have been proposed to approximate the Reynolds stresses. The central ides in most of the turbulence models, except the Reynolds-stress model or algebraic stress modeling, is the employment of artificial turbulent viscosity μ_t to account for the additional diffusional flux due to the turbulent motion. To do that, the Reynolds stress term in Eq. 3.7 is expressed as

$$-\rho\overline{u_i u_j} = \mu_t\left(\frac{\partial U_i}{\partial x_j} + \frac{\partial U_j}{\partial x_i}\right) - \frac{1}{3}\rho\delta_{ij}\,\overline{u_k u_k} \quad . \tag{4.1}$$

where μ_t is the turbulent viscosity. It is a property of the local state of turbulence, not a property of the fluid. The turbulence model in this category is generally referred to as a viscosity model.

In Eq. 4.1, the only problem that remains to be solved is the derivation of turbulent viscosity μ_t. The following section will describe the derivation of μ_t in three different turbulence models (2-equation, 1-equation and 0-equation).

4.1 2- EQUATION (k-ε) MODEL

In the k-ε model, turbulent viscosity μ_t is computed from the relation

$$\mu_t = \frac{C_\mu \rho k^2}{\varepsilon} \quad . \tag{4.2}$$

Here, C_μ is a constant having the recommended value 0.09,

$$k = \frac{1}{2}\,\overline{u_i u_i} \tag{4.3}$$

is the turbulence kinetic energy,

$$\varepsilon = \nu\,\overline{\frac{\partial u_i}{\partial x_j}\frac{\partial u_i}{\partial x_j}} \tag{4.4}$$

is the dissipation rate of turbulent kinetic energy and ν is the kinematic viscosity. In this model, we first solve the transport equations of k and ε (Sec. 5) and then compute the turbulent viscosity μ_t from Eq. 4.2.

4.2 1-EQUATION (k) MODEL

In the 1-equation (k) model, the turbulent viscosity is computed also from Eq. 4.2 as in the k-ε model. However, instead of solving the transport equation for ε, we calculate it using the relation

$$\varepsilon = \frac{C_\mu^{3/4}\, k^{3/2}}{\ell} \quad . \tag{4.5}$$

Here, the length scale ℓ is related to the distance y from the wall as

$$\ell = \kappa y \quad . \tag{4.6}$$

In Eq. 4.6, κ is the von Karman constant and its recommended value is 0.42.

In the case of multidimensional flow with more than one wall co-existing, the value of y, used to compute ℓ, is the nearest distance from a wall. In addition, a cutoff value of y is either 0.175 D_H or a preassigned length, where D_H is the hydraulic diameter.

4.3 0-EQUATION MIXING-LENGTH MODEL

In the 0-equation mixing-length model, the turbulent viscosity is computed from the relation

$$\mu_t = \rho \ell^2 \left[\frac{\partial U_i}{\partial x_j} \left(\frac{\partial U_i}{\partial x_j} + \frac{\partial U_j}{\partial x_i} \right) \right]^{1/2} . \tag{4.7}$$

The mixing length ℓ is evaluated in the same way as in the 1-equation (k) model ($\ell = \kappa y$). In the 0-equation mixing-length model, we do not solve any transport equation of turbulence quantities.

4.4 TURBULENT DIFFUSIVE FLUX FOR ENERGY EQUATION

In the energy equation, to account for the extra rate of enthalpy transport due to the turbulence fluctuations, the turbulent thermal conductivity, λ_t, is computed from

$$\lambda_t = \frac{\mu_t C_p}{\sigma_h} . \tag{4.8}$$

In Eq. 4.8, C_p is the specific heat of a fluid and σ_h is the turbulent Prandtl number for thermal energy transfer. The recommended value for σ_h is 0.9.

5. TRANSPORT EQUATIONS OF 2-EQUATION (k-ε) MODEL

In the 2-equation (k-ε) model, as mentioned earlier, we need to know the values of k and ε to determine the turbulent viscosity μ_t. We present here the derivation of two sets of governing differential equations designated as high-Reynolds-number flow model and low-Reynolds-number flow model.

5.1 HIGH REYNOLDS NUMBER FLOW MODEL

5.1.1 Transport Equation for k

We first subtract Eq. 3.7 from Eq. 3.2 to obtain

$$\rho \left(\frac{\partial u_i}{\partial t} + U_j \frac{\partial u_i}{\partial x_j} \right) = - \frac{\partial p}{\partial x_i} - \rho u_j \frac{\partial U_i}{\partial x_j} - \frac{\partial}{\partial x_j} \left(\rho u_i u_j - \rho \overline{u_i u_j} \right)$$

$$+ \frac{\partial}{\partial x_j} \mu \left(\frac{\partial u_i}{\partial x_j} + \frac{\partial u_j}{\partial x_i} \right) + \rho' g_i , \tag{5.1}$$

where ρ' denotes the turbulent density fluctuation and p is the fluctuation in static pressure. In this study, $\rho' = -\rho\beta T'$, where β is the volumetric coefficient of expansion and T' is the fluctuating temperature.

After multiplying by u_i, time-averaging Eq. 5.1, and using the definition $k = \frac{1}{2}\overline{u_i u_i}$, we obtain

$$\rho \frac{\partial k}{\partial t} + U_j \frac{\partial k}{\partial x_j} = -\rho\overline{u_i u_j}\frac{\partial U_i}{\partial x_j} + \overline{\rho' u_i} g_i - \mu \overline{\frac{\partial u_i}{\partial x_j}\left(\frac{\partial u_i}{\partial x_j} + \frac{\partial u_j}{\partial x_i}\right)}$$

$$\text{A} \qquad \text{B} \qquad \text{C}$$

$$+ \frac{\partial}{\partial x_j}\left[\mu\left(\frac{\partial k}{\partial x_j} + \frac{\partial \overline{u_i u_j}}{\partial x_i}\right) - \rho\,\overline{\frac{u_i u_i u_j}{2}} - \overline{p u_i}\,\delta_{ij}\right]. \qquad (5.2)$$

$$\text{D}$$

Equation 5.2 is the exact form of the transport equation for k. Here, the terms are

A : source due to mean shear,

B : buoyancy interactions,

C : loss of k through viscous dissipation, and

D : diffusive transport of k and randomizing action of the pressure-strain correlation.

We can see that Eq. 5.2 has the closure problem. After adoption of the gradient-transport notion[14], Eq. 5.2 may be written as

$$\rho \frac{\partial k}{\partial t} + \rho\, U_j \frac{\partial k}{\partial x_j} = P_k + G_k - \rho\varepsilon + \frac{\partial}{\partial x_j}\left[\left(\frac{\mu_t}{\sigma_k} + \mu\right)\frac{\partial k}{\partial x_j}\right]. \qquad (5.3)$$

Here,

$$P_k = \mu_t\left[\frac{\partial U_i}{\partial x_j}\left(\frac{\partial U_i}{\partial x_j} + \frac{\partial U_j}{\partial x_i}\right)\right] \qquad (5.4)$$

is the source due to mean shear and

$$G_k = -\frac{\mu_t}{\rho\sigma_h}\frac{\partial \rho}{\partial T}\left(\frac{\partial T}{\partial x_j} g_j\right) \qquad (5.5)$$

is due to thermal stratification. The term containing σ_k in Eq. 5.3 represents the diffusion of k. σ_k is called the turbulent Prandtl number for k. The recommended value[12] for σ_k is 1.0.

5.1.2 Transport Equation for ε

The exact form of the transport equation for ε is obtained by taking the derivative of Eq. 4.1, with respect to x_j, and multiplying it by

$$2\nu\left(\frac{\partial u_i}{\partial x_j}+\frac{\partial u_j}{\partial x_i}\right).$$

The resulting equation is discussed in detail, by Daly and Harlow[16], Hanjalic and Launder[11], and Lumley and Khajeh-Nouri[17]. The only feasible approach toward devising an ε equation is to apply both intuition and intelligent dimensional analysis. The ε equation contains several empirical coefficients that require adjusting to account for different behaviors of different shear flows. The equation proposed by Jones and Launder[10] and Daly and Harlow[17] is

$$\rho\frac{\partial\varepsilon}{\partial t}+\rho U_j\frac{\partial\varepsilon}{\partial x_j}=C_1\frac{\varepsilon}{k}(P_k+G_k)-C_2\frac{\rho\varepsilon^2}{k}+\frac{\partial}{\partial x_j}\left[\left(\frac{\mu_t}{\sigma_\varepsilon}+\mu\right)\frac{\partial\varepsilon}{\partial x_j}\right]. \qquad (5.6)$$

Here, the source term P_k has the same form as Eq. 5.4; the second term on the right is the dissipation term, and the last term represents diffusion. The variable σ_ε is the turbulent Prandtl number for ε, the recommended value[14] is 1.3. The coefficient of the production term, C_1, is normally chosen by reference to near-wall turbulence, whereas the coefficient C_2 is determined from the decay of grid turbulence. The recommended values of C_1 and C_2 by Launder et al.[19] are 1.44 and 1.92, respectively.

5.2 LOW REYNOLDS-NUMBER FLOW MODEL

In the 2-equation (k-ε) turbulence model for high Reynolds number flow (Sec. 5.1), the low Reynolds number effects are assumed negligible. Consequently, the special treatment, called wall function (Sec. 6.3), is required for the near-wall regions where the low Reynolds number effects are not negligible. In addition, the high Reynolds number flow model is not suitable for the analysis of problems wherein the mean flow Reynolds number is low.

To remedy these deficiencies, Jones and Launder[10,18] have developed a low Reynolds number version of the 2-equation (k-ε) model. This low Reynolds number flow model is applicable in the entire flow domain and does not require separate wall function treatment for near-wall regions.

The transport equations for k and ε of the low Reynolds number model of Jones and Launder[10,18] are:

$$\rho\frac{\partial k}{\partial t}+\rho U_j\frac{\partial k}{\partial x_j}=P_k+G_k-\rho\varepsilon+\frac{\partial}{\partial x_j}\left[\left(\frac{\mu_t}{\sigma_k}+\mu\right)\frac{\partial k}{\partial x_j}\right]-2\mu\left(\frac{\partial k^{1/2}}{\partial x_j}\right)\left(\frac{\partial k^{1/2}}{\partial x_j}\right) \qquad (5.7)$$

and

$$\rho \frac{\partial \varepsilon}{\partial t} + \rho U_j \frac{\partial \varepsilon}{\partial x_j} = C_1 \frac{\varepsilon}{k}(P_k + G_k) - f_2 \frac{\rho \varepsilon^2}{k} + \frac{\partial}{\partial x_j}\left[\left(\frac{\mu_t}{\sigma_\varepsilon} + \mu\right)\frac{\partial \varepsilon}{\partial x_j}\right]$$

$$+ C_3 \frac{\mu \mu_t}{\rho}\left(\frac{\partial^2 U_i}{\partial x_j \partial x_\ell}\right)\left(\frac{\partial^2 U_i}{\partial x_j \partial x_\ell}\right). \qquad (5.8)$$

The turbulent viscosity is computed as

$$\mu_t = f_\mu \frac{\rho k^2}{\varepsilon}. \qquad (5.9)$$

The constant, C_3, in Eq. 5.8 has the recommended value of 2.0. The functions f_μ and f_2 are

$$f_\mu = C_\mu \exp\left[-2.5/(1 + R_t/50)\right] \qquad (5.10)$$

and

$$f_2 = C_2 \left[1.0 - 0.3 \exp(-R_t^2)\right]. \qquad (5.11)$$

Here, R_t is the turbulence Reynolds number, defined as

$$R_t = \frac{\rho k^2}{\mu \varepsilon}. \qquad (5.12)$$

The constants C_μ, C_1, C_2, σ_k, and σ_ε have the same value as the high-Reynolds-number k-ε model. If R_t is much greater than 1, f_μ approaches C_μ and f_2 approaches C_2.

The additional term

$$-2\mu\left(\frac{\partial k^{1/2}}{\partial x_j}\right)\left(\frac{\partial k^{1/2}}{\partial x_j}\right),$$

in the k-equation in the low-Reynolds number model, increases the computational stability of k-equation[19]. In the equation for ε, the term

$$C_3 \frac{\mu \mu_t}{\rho}\left(\frac{\partial^2 U_i}{\partial x_j \partial x_\ell}\right)\left(\frac{\partial^2 U_i}{\partial x_j \partial x_\ell}\right)$$

in Eq. 5.8 is included to account for the increasing importance of the laminar diffusive transport.

It may be emphasized here that for a low-Reynolds-number model, no special treatment for near-wall regions (Sec. 6.3) is required. However, in order to improve the results of numerical computation, fine mesh may be required in the regions near a solid wall.

6. BOUNDARY CONDITIONS

There are three types of boundaries:

A line or surface (plane) of symmetry,

Inlet and outlet boundaries, and

A solid wall.

These boundaries are discussed in the following sections.

6.1 SYMMETRY BOUNDARY

The simplest boundary is the line or plane of symmetry; at a symmetry line, the normal velocity is set to zero. The gradients of scalar normal to the symmetry line also are set to zero.

6.2 INLET AND OUTLET BOUNDARIES

At the outlet plane (free boundary), the gradient of turbulence quantities are assumed to be zero. The inlet plane requires special treatment. The inlet turbulence kinetic energy k_{in}, can be obtained from the measurement if it is available.

For the uniform inlet velocity U_{in}, k_{in} can be estimated as follows:

$$k_{in} = 0.001 U_{in}^2 . \tag{6.1}$$

The inlet dissipation rate of turbulence kinetic energy ε_{in} is

$$\varepsilon_{in} = \frac{C_\mu^{3/4} k_{in}^{3/2}}{\ell} , \tag{6.2}$$

where ℓ_{in} is the length scale at inlet.

If the profile of mean velocity at inlet plane is known or can be guessed, k_{in} is estimated from

$$k_{in} = 3\ell_{in}^2 \left[\left(\frac{\partial U}{\partial y} \right)^2 + \left(\frac{\partial U}{\partial z} \right)^2 \right] . \tag{6.3}$$

U is the mean velocity component in the main flow direction. ε_{in} is computed from Eq. 6.2.

6.3 WALL-FUNCTION TREATMENT

In the immediate vicinity of a solid wall, there is a large variation in the values of turbulence properties. Therefore, to predict the correct values of momentum flux, energy flux, and the gradients of k and ε, we apply a special treatment called the wall-function treatment. In this procedure, we implicitly account for steep variation near a wall and avoid the need of using

a fine mesh. This procedure is described here briefly; more detailed information can be found in Sha and Launder[14].

6.3.1 Wall Shear Stress in the Momentum Equation

The illustration of the model used for a near wall region is shown in Fig. 1. P is the node adjacent to the wall and outside of the viscosity-affected zone (viscous sublayer), NP is the node next to P, and the distance y_p is the distance from P to the wall. The sublayer thickness y^* is determined such that the Reynolds number R_t^* at the edge of the region is ~ 20.

$$R_t^* \equiv \frac{y^* k^{*1/2}}{\nu} = 20 \ . \tag{6.4}$$

The level of turbulent kinetic energy k^* at y^* is obtained by linearly extrapolating the values of k_p and k_{NP} to $y = y^*$:

$$k^* = k_p + \frac{y_p - y^*}{y_{NP} - y_p} \left(k_p - k_{NP} \right) \ . \tag{6.5}$$

Based on the assumption of logarithmic velocity profile from turbulent Couette flow, the wall shear stress between the node P and the wall is modified to account for the frictional force at the wall. The modified wall shear stress, in lieu of the normally calculated value, is

$$\tau_w = \frac{\rho k_p^{1/2} U_p \kappa C_\mu^{1/4}}{\ell n \left(\frac{E y_p C_\mu^{1/4} k_p^{1/2}}{\nu} \right)} \tag{6.6}$$

which is deduced from the velocity profile

$$\frac{U_p}{\tau_w/\rho} k_p^{1/2} = C_\mu^{-1/4} \frac{1}{\kappa} \ell n \left(\frac{E y_p C_\mu^{1/4} k_p^{1/2}}{\nu} \right). \tag{6.7}$$

The constant E has the value of 9.0 and U_p is the velocity parallel to the wall at node P. The shear stress calculated from Eq. 6.6 is assumed invariant from node P to the wall.

6.3.2 Wall Heat Flux in the Energy Equation

In the energy equation, the heat flux near the wall is modified using a logarithmic temperature profile. The modification for the wall heat flux is similar to that made for the wall shear stress in the momentum equation except that an additional term is introduced to include the resistance of the laminar sublayer. For the case of a laminar Prandtl number $\sigma_{h,\ell}$ of the order of 1 or greater, the wall heat flux is

$$q_w = \frac{\rho k_p^{1/2} C_\mu^{1/4} (h_w - h_p)}{\frac{1}{\kappa} \ell n \left(\frac{E y_p C_\mu^{1/4} k_p^{1/2}}{\nu} \right) + P_f} , \tag{6.8}$$

where

$$P_f = 9.24 \left(\frac{\sigma_{h,\ell}}{\sigma_h} - 1 \right) \left(\frac{\sigma_h}{\sigma_{h,\ell}} \right)^{1/4} . \tag{6.9}$$

In Eq. 6.8, h is the enthalpy and subscripts w and P represent the values at wall and node P, respectively. P_f is generally referred to as P-function and σ_h is the turbulent Prandtl number for thermal energy transfer, as defined previously.

For the case of a low Prandtl number, such as liquid metal flow where $\sigma_{h,\ell}$ is in the order of 10^{-2}, the turbulence contribution to the wall heat flux is small. The temperature profile between the wall and node P can be assumed linear.

6.3.3 Turbulence Quantities k and ε Near a Solid Wall

For treatment of the transport equation of k, the diffusive flux from node P to the wall is first set to zero. The production term P_k in the k equation is modified as

$$P_k = \tau_w U_p / y_p ; \tag{6.10}$$

instead of using mean shear, τ_w is the modified wall shear stress computed from Eq. 6.6.

In the transport equation of ε, the dissipation rate at node P is computed as

$$\varepsilon_p = \frac{C_\mu^{3/4} k_p^{3/4}}{\ell} , \tag{6.11}$$

instead of solving the transport equation for ε. In addition, the average value of ε is computed by integrating the nonlinear variation of ε for the near-wall cell. Thus,

$$\bar{\varepsilon} = \frac{1}{y_e} \int_0^{y_e} \varepsilon dy$$

$$= \frac{C_\mu^{3/4} k_p^{3/2}}{\kappa y_e} \ell n \left(\frac{E y_e C_\mu^{1/4} k_p^{1/2}}{\nu} \right), \tag{6.12}$$

where y_e is the value at the edge of control volume of node P as shown in Fig. 1. The value of ε is used to evaluate the dissipation term in the equation for k for the near-wall cell.

7. NUMERICAL SIMULATIONS

To validate the new turbulence models in COMMIX, we have performed several numerical simulations and compared the results with the experimental data. The results of the following three numerical simulations are presented in this section.

- Isothermal turbulent flow in a pipe,
- Isothermal turbulent flow in a duct with abrupt expansion.
- Thermal and fluid mixing in the cold leg and downcomer of a pressurized water reactor.

7.1 TURBULENT FLOW IN A PIPE

7.1.1 Problem Description

The developing turbulent flow in the inlet region of a straight pipe is the first problem considered in the validation of turbulence modeling by the COMMIX code. The Reynolds number ($Re = \rho w_o D/\mu$) is 3.38×10^5 where D is the diameter of the pipe and w_o is the uniform mean velocity at the inlet. The measurements of axial velocity profile at various locations were performed by Barbin and Jones[20].

7.1.2 Solution Procedure

In our computation, a 2-D axisymmetric flow is assumed and 1000 cells (20 in the radial direction and 50 in the axial direction) are used. Because the inlet condition for k and ε were not reported, the assumptions based on the uniform inlet velocity at the inlet as described in Sec. 6, were applied. The fully implicit numerical scheme was used. Three different simulations were performed using the following turbulence models:

- 2-equation (k-ε) model.
- 1-equation (k) model with maximum cut-off length scale = $0.175\,\kappa D_H$.
- Constant turbulent viscosity model with $\mu_t = 500\,\mu$.

7.1.3 Results and Discussion

The development of axial velocity profile at two different axial locations (z/D = 16.5 and z/D = 40.5, z being the axial distance) with different turbulence models are shown in Fig. 2. The predictions of the 2-equation (k-ε) model are in very good agreement with measurement. Because the separated flow does not exist, the predictions of the 1-equation (k) model with cut-off length scale $\ell_{max} = 0.175\,\kappa D_H$, D_H being the pipe diameter D, is also in good agreement with measurement. In the constant turbulent viscosity model, the axial velocity profile approaches, as expected, the fully developed parabolic profile at z/D = 40.5.

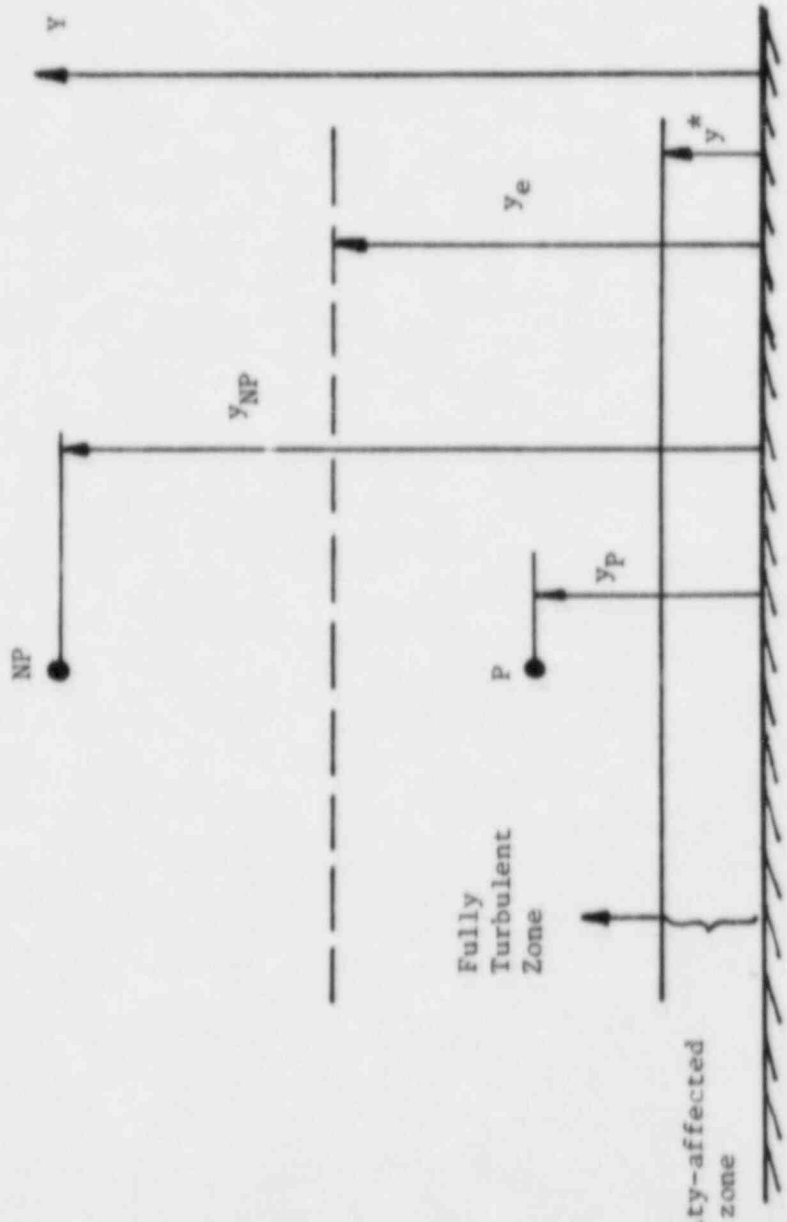

Fig. 1. Model of a Near-Wall Region

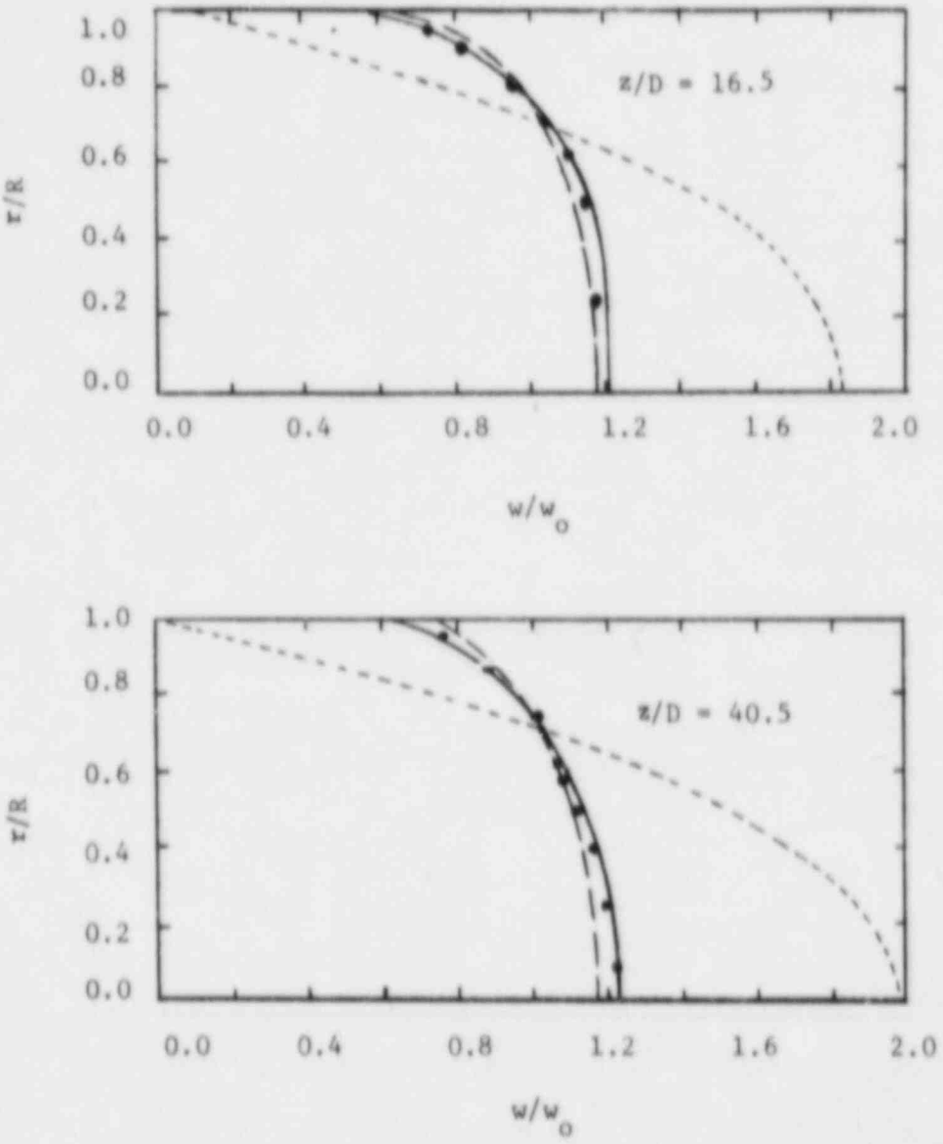

Data from Barbin and Jones Ref. 20

——— Predictions of (k-ε) Model

— — Predictions of 1-equation Model ($\ell_{max} = 0.175\ \kappa D_H$)

----- Predictions of constant turbulent viscosity ($\mu_t = 500\ \mu$)

Fig. 2 Development of Velocity Profile at Two Axial Locations in a Pipe (Re = 338,000).

7.2 FLOW IN A CIRCULAR DUCT WITH SUDDEN EXPANSION

7.2.1 Problem Description

An isothermal fluid with uniform velocity w_o enters a circular duct, having abrupt expansion $r_o/r_i = 2$, as shown in Fig. 3. The operating conditions in the Chaturvedi's experiment[21] are:

Fluid	: Air.
Inlet velocity (w_o)	: 30.48 m/s.
Inner radius (r_i)	: 0.054 m.
Outer radius (r_o)	: 0.108 m.
Reynolds number ($Re_{r_i} = \frac{2\rho w_o r_i}{\mu}$)	: 2.186×10^5.
Temperature	: Constant.

The inlet conditions were not reported by Chaturvedi but were assumed to be:

Temperature	: 25°C.
Inlet turbulent kinetic energy (k_{in})	: $0.001\ w_o^2$.
Inlet Dissipation Rate of Turbulence Energy (ε_{in})	: $\frac{C_\mu^{3/4}\ k_{in}^{3/2}}{\ell_{in}}$.

We selected this problem for presentation here because:

- Experimental measurements are available,
- A turbulence model is needed to analyze complex recirculating flow downstream of expansion, and
- It will demonstrate that a 2-equation (k-ε) turbulence model provides better prediction of separated flow.

7.2.2 Solution Procedure

Due to axisymmetry, the flow is two-dimensional. We used a total of 500 cells (10 in r-direction x 50 in z-direction) to model the geometry. The COMMIX-1A fully-implicit numerical scheme was used to analyze the problem. Four different simulations were performed, using the following turbulence models:

- Constant turbulent viscosity ($\mu_t = 500\ \mu$),
- 0-equation mixing length model,
- 1-equation (k) model (cut-off length scale = $0.175\ \kappa r_o$), and
- 2-equation (k-ε) model.

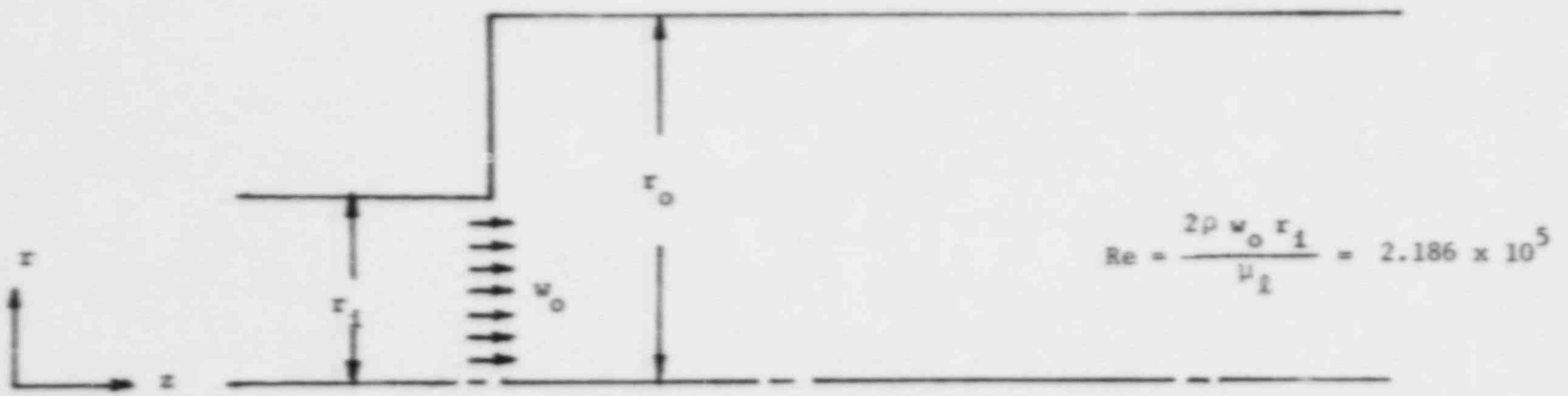

Fig. 3. Model Geometry of Isothermal Turbulent Flow in a Sudden Expansion ($r_o/r_i = 2.0$)

7.2.3 Results and Discussion

The calculated and experimental mean velocity profiles at three downstream locations (z/r_o = 1.0, 3.0, and 8.0) are compared in Fig. 4. We can see the following from these comparisons:

- The 2-equation (k-ε) model has the best agreement with experimental data; the maximum difference is less than 10% (except for the region near the wall). Agreement is extremely good at z/r_o = 8.0.
- The predictions of the 0-equation mixing-length and 1-equation-k models are not as good as those of the 2-equation (k-ε) model; they may be considered as marginally acceptable in the entrance region (z/r_o = 1, 3) but become poorer in the far downstream region.
- The predictions of the constant-turbulent-viscosity model have a far downstream velocity profile close to the parabolic profile (laminar), as they should.
- The 2-equation (k-ε) model is needed to correctly predict highly secondary flow.
- The 2-equation (k-ε) model predictions are closer to experimental data than those of the 1-equation (k) model.
- Inside the recirculating zone, the predictions of both the 2-equation (k-ε) and 1-equation (k) models are not as good. This may be because the present turbulence models are based on the assumption that turbulence is isotropic. In the recirculating zone, the eddies are very strong and the assumption of isotropy will not hold.
- Far downstream, where the eddies are not very strong, the predictions of the 2-equation (k-ε) model are in very close agreement.

The comparisons of turbulent intensities at three axial locations are presented in Fig. 5. The vector plot, showing the velocity field based on the 2-equation (k-ε) model, is presented in Fig. 6. We can see a recirculating zone downstream of expansion. As the flow progresses downstream, the recirculating eddies gradually disappear.

7.3 THERMAL AND FLUID MIXING IN THE COLD LEG AND DOWNCOMER OF A PWR

7.3.1 Problem Description

So far, very few applications of turbulence models have been made for the analysis of nonisothermal transient flows; most applications are limited to steady isothermal flows. The example we have considered here is a transient computation involving thermal and fluid mixing in the cold leg and downcomer of a PWR. This problem has an important application to the pressurized thermal shock issue, which has an urgent safety issue in the nuclear industry.

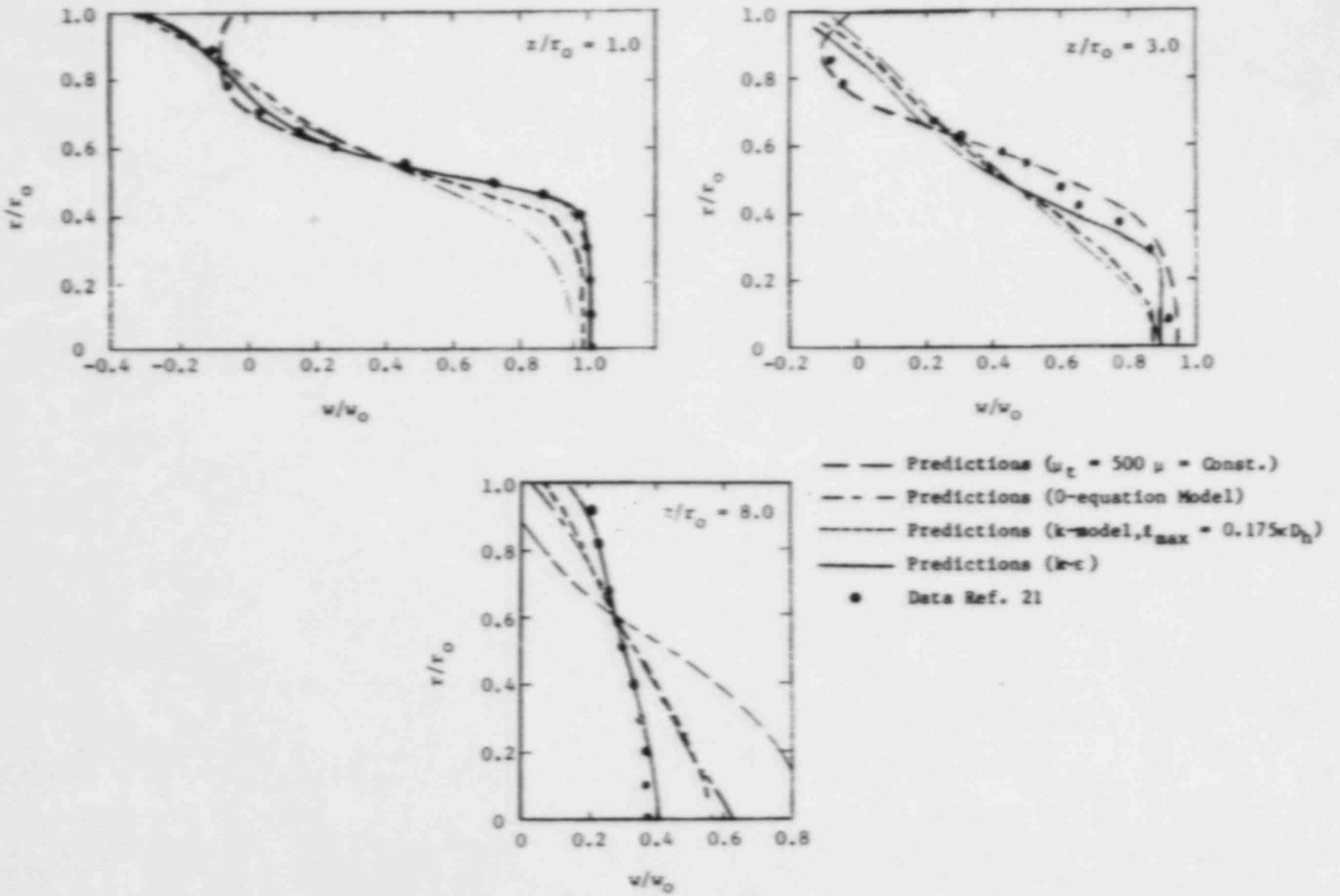

Fig. 4 Axial Velocity Profiles Downstream of a Sudden Expansion

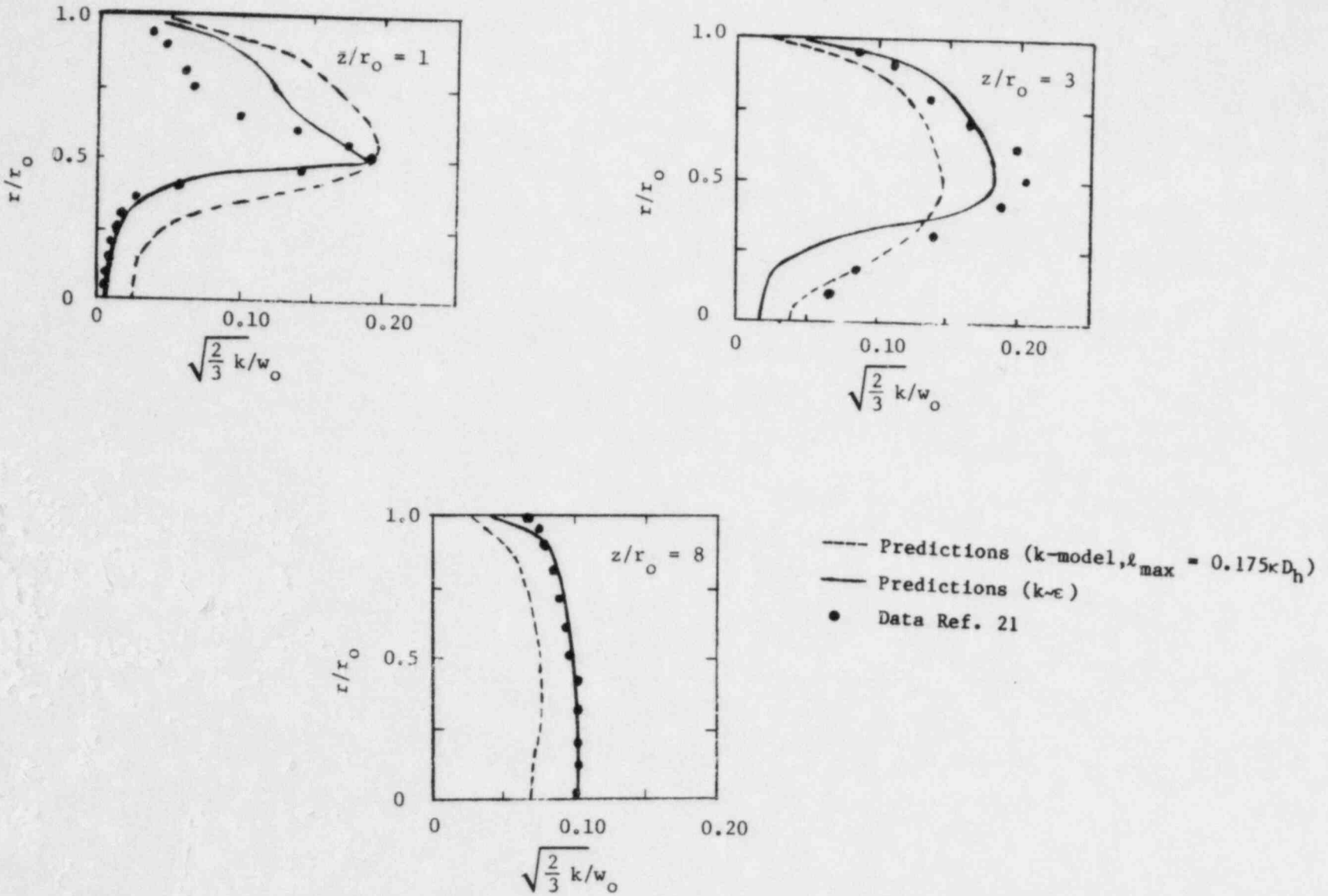

Fig. 5 Normalized Fluctuating Energy Downstream of a Sudden Expansion

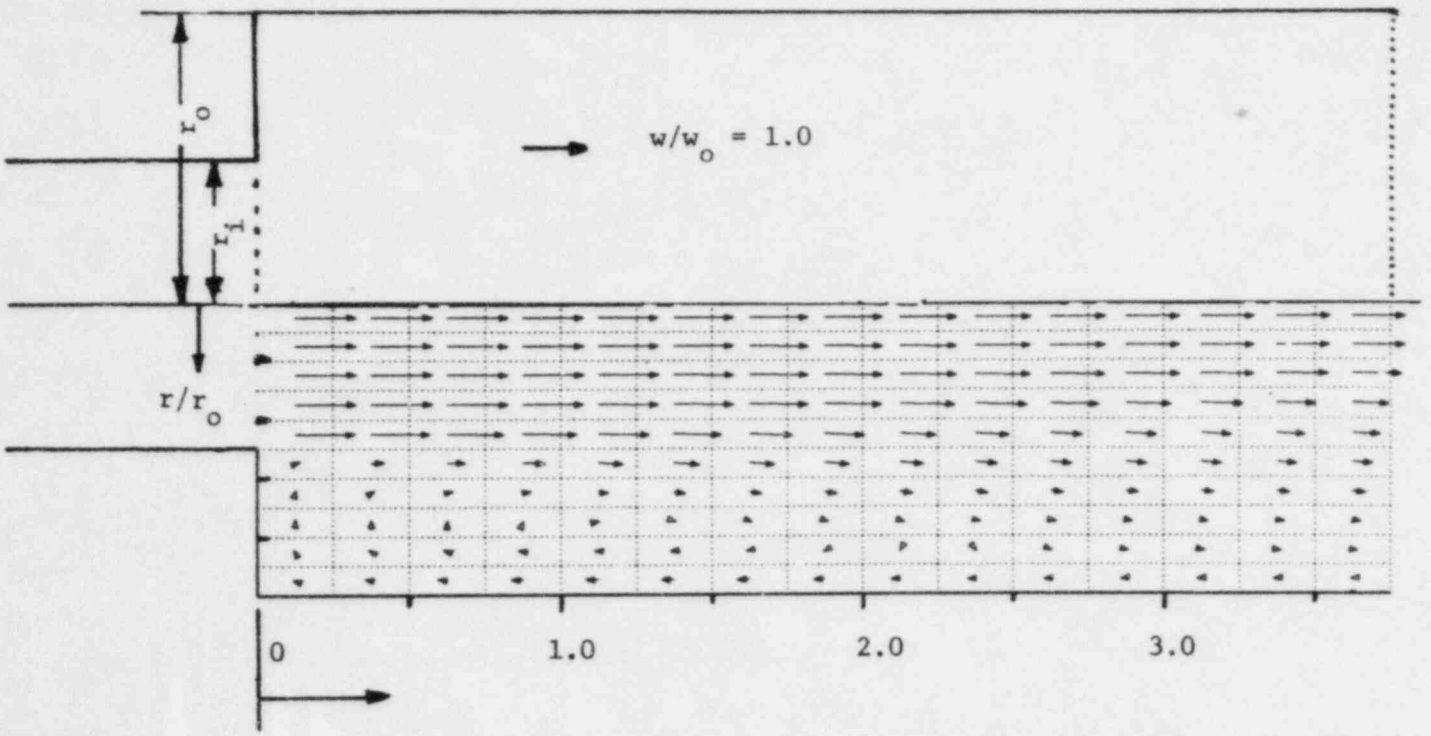

Fig. 6 Vector Plot of Isothermal Turbulent Flow in a Sudden Expansion ($r_o/r_i = 2.0$, $Re_{ri} = 2.186 \times 10^5$)

Figure 7 illustrates the geometry of the cold leg and downcomer used in the EPRI-SAI thermal and fluid mixing experiment[22]. The objective of the experiment was to investigate the buoyancy-driven thermal mixing in a geometry simulating PWR. The cross-sections of both the downcomer and cold leg are rectangular. The small dots in the cold leg in Fig. 7 represent the locations of thermocouples used in the experiment.

In the experiment, loop flow enters the cold leg at 70°C and flows down the cold leg to the downcomer. Approximately one-fifth of the way down from the entrance, a cold fluid at 17°C from High-Pressure Injection (HPI) enters the cold leg at an angle of 60°, as shown in Fig. 7. At the injection section, the cold fluid is at the top resulting in an unstable thermal stratification*. As both fluids flow down the cold leg, cold fluid slowly penetrates to the bottom of the cold leg before it reaches the downcomer. Complete penetration of the cold fluid to the bottom results in what is known as stable thermal stratification*. Near the downcomer, a further increase in thermal stratification occurs as some of the hot stagnant fluid (70°C) from the downcomer is sucked into the cold leg. The test conditions and relevant parameters are summarized in Table 1.

In the experiment, there were variations in flow rates and temperatures of the cold leg and HPI, and there were heat losses from the walls of the test section. But, in our analysis, these are assumed to be negligible.

7.3.2 Solution Procedure

7.3.2.1 Modeling

In our analysis, we assumed a symmetry with respect to the central plane (y=0); therefore, only half of the geometry was modeled. We used a total of 1290 cells (IMAX=30; JMAX=8; KMAX=27) to model the half geometry. The angled HPI injector and diffusing nozzle portions of the cold leg were modeled using the concept of irregular cells instead of using a conventional zig-zag approximation.

7.3.2.2 Four Simulations

Four numerical simulations were performed, using the following turbulence models.

Case 1: Constant turbulence viscosity model (μ_t = 0.06 pa-s). This is included only for comparison.

Case 2: 1-equation (k) model.

Case 3: 2-equation (k-ε) model without Volume-Weighted Skew-Upwind Difference (VWSUD) scheme.

---

* Stable thermal stratification is continuously increasing temperature from bottom to top; unstable thermal stratification is having some cold fluid above the hot fluid.

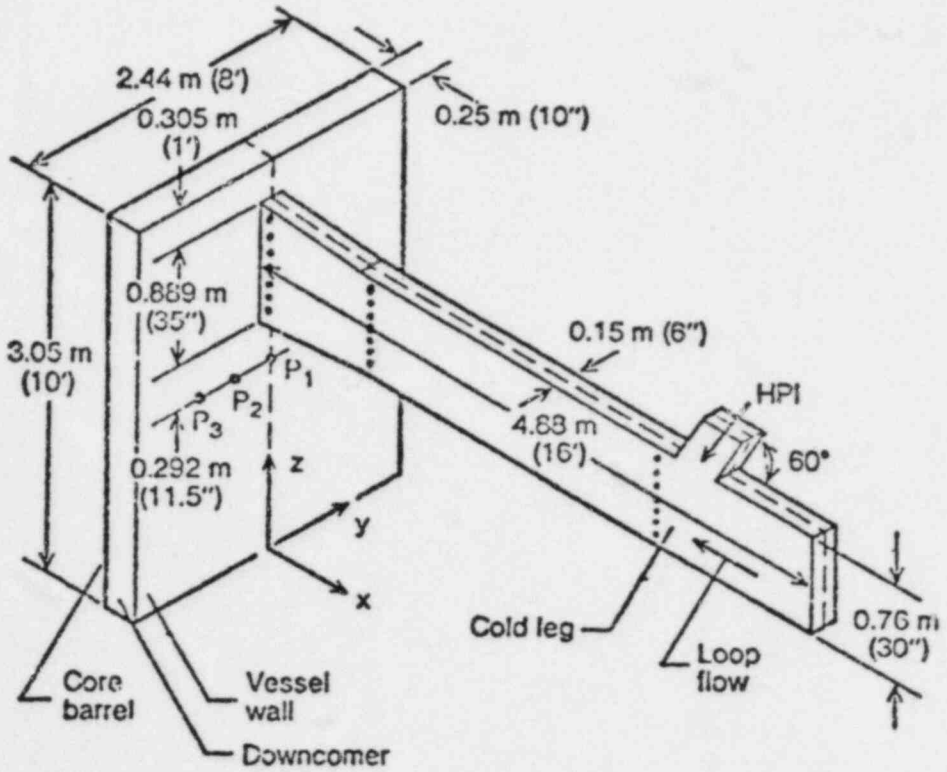

Fig. 7. Model Geometry of Cold Leg and Downcomer used in SAI Thermal and Fluid Mixing Test ('.' indicates thermocouple location).

Table 1. Summary of Test Conditions and Relevant Parameters for Test 1 of SAI Full Weight Thermal Mixing Experiment

Parameter	Value
Average flow rate of cold leg	10.6 ℓ/s (168.5 gpm)
Average flow rate of HPI (after injection)	1.0 ℓ/s (16 gpm)
Inlet temperature of cold leg	70°C
Inlet temperature of HPI (after injection)	17°C
Ratio of loop flow rate to HPI flow rate	10.6
Inlet velocity of cold leg	0.0913 m/s
Inlet velocioty of HPI	0.0258 m/s
$Re_{CL} = \frac{\rho_{CL} V_{CL} D_{CL}}{\mu_{CL}}$	3.8×10^4
$Fr_{CL} = \frac{V_{CL}}{g D_{CL} \frac{\rho_{HPI} - \rho_{CL}}{(\rho_{HPI} + \rho_{CL})/2}}$	0.44
$Fr_{MIX} = \frac{V_{HPI} \frac{A_{HPI}}{A_{CL}}}{g D_{CL} \frac{\rho_{HPI} - \rho_{CL}}{\rho_{HPI}}}$	0.04

Case 4: 2-equation ($k-\varepsilon$) model with Volume-Weighted Skew-Upwind Difference Scheme.

The numerical simulations were performed using the fully implicit numerical scheme.

Prior to the initiation of HPI, isothermal steady-state conditions were obtained. After that, the HPI was introduced at time t = 0, and the transient computations were performed.

7.3.2.3 Basis of Four Simulations

Case 1 is performed only for comparison purposes. Cases 2 and 3 are simulations with the 1-equation (k) model (Case 2) and 2-equation ($k-\varepsilon$) model (Case 3).

Recently, we implemented a Volume-Weighted Skew-Upwind Difference (VWSUD) scheme to reduce the magnitude of numerical diffusion. Case 4 is the simulation with the 2-equation ($k-\varepsilon$) model with Volume-Weighted Skew-Upwind Difference (VWSUD) scheme.

7.3.3 Comparison with Experiment

The comparisons of vertical temperature profiles at the junction of straight and diverging sections of the cold leg and the junction of cold leg and downcomer are presented in Tables 2 and 3, respectively.

7.3.3.1 Discussion of Results in Table 2

In Table 2, thermocouples L36 through L42 represent temperature readings from top to bottom. From this comparison, we can see that at the junction of straight and diverging sections of the cold leg:

- Experimental data show a stable thermal stratification; cold fluid from HPI has completely penetrated to the bottom of the cold leg.
- The temperature profile from the base case (Case 1) is nearly uniform, showing no stratification, and complete mixing.
- The 1-equation (k) model (Case 2) shows stratification, but cold fluid has not been able to penetrate completely down to the bottom of the cold leg.
- The 2-equation ($k-\varepsilon$) model (Case 3) predicts stable thermal stratification and the results are in reasonable agreement with the experimental data.
- The 2-equation ($k-\varepsilon$) model with VWSUD (Case 4) predicts stable thermal stratification and the results are in good agreement with the experimental data.

7.3.3.2 Discussion of Results in Table 3

In Table 3, thermocouples L43 through L49 represent temperature readings from top to bottom.

Table 2. Comparison of Temperature Profiles at Junction of Straight and Diverging Sections of Cold-Leg (Time = 119 sec after Initiation of HPI)

Location (Thermocouple #)	Experiment	Base Model (μ_t = 0.06 pa-s)	k-ε Model without VWSUD	k-ε Model with VWSUD	1-Equation (k) Model without VWSUD
L36 (Top)	65.6°C	63.5°C	63.5°C	64.9°C	60.7°C
L37	65.8°C	64.0°C	64.2°C	65.1°C	61.9°C
L38	65.3°C	64.1°C	64.4°C	65.0°C	63.9°C
L39	64.3°C	64.1°C	64.4°C	64.8°C	66.4°C
L40	64.6°C	64.1°C	64.3°C	64.5°C	68.6°C
L41	*	64.0°C	64.2°C	64.1°C	69.8°C
L42 (Bottom)	62.3°C	64.1°C	64.1°C	63.8°C	69.9°C

* No reading reported.

Table 3. Comparison of Temperature Profiles at Junction of Cold Leg and Downcomer (time = 119 sec after initiation of HPI)

Location (Thermocouple #)	Experiment	Base Model (μ_t = 0.06 pa-s)	k-ε Model without VWSUD	k-ε Model with VWSUD	1-Equation (k) Model without VWSUD
L43 (Top)	*	66.3°C	69.5°C	69.6°C	68.1°C
L44	68.3°C	65.4°C	66.3°C	66.9°C	63.6°C
L45	64.3°C	64.9°C	65.4°C	65.9°C	63.0°C
L46	64.1°C	64.7°C	65.0°C	65.4°C	63.5°C
L47	62.2°C	64.5°C	64.8°C	65.0°C	64.7°C
L48	64.3°C	64.4°C	64.6°C	64.6°C	66.1°C
L49 (Bottom)	64.4°C	64.3°C	64.4°C	64.1°C	67.1°C

*No reading reported.

At the junction of the cold leg and downcomer, if the buoyancy force is sufficiently large, we can have recirculation, which increases thermal stratification--cold fluid at the bottom of the cold leg moves toward the downcomer and hot stagnant fluid is sucked from the downcomer into the top of the cold leg. Such a recirculating phenomenon was observed through flow visualization in the experiment[22,23].

We see from Table 3 that at this junction:

- The 2-equation (k-ε) model (Cases 3 and 4) predicts stable thermal stratification with temperatures in close agreement (except at Thermocouple L47) with experimental data.
- Although the base model (Case 1) predicts stable thermal stratification, the degree of stratification is small compared with the experiment.
- The 1-equation (k) model (Case 2) has the worst temperature profile prediction. Cold fluid has not penetrated completely to the bottom of the cold leg.

7.3.3.3 Transient Temperatures

From the results discussed in Secs. 7.3.3.1 and 7.3.3.2, it is clear that the predictions of the 2-equation (k-ε) model are better than those of the 1-equation (k) and constant turbulent viscosity models. Although the addition of volume-weighted skew-upwind differencing improves the numerical predictions, the results obtained by using the 2-equation (k-ε) model only (Case 3) are presented and discussed here to demonstrate the effect solely due to turbulence modeling.

The comparison of the calculated and experimental temperature profiles at three vertical sections during the transient, are shown in Figs. 8-10. Figure 8 is the transient temperature plot at the junction of the downcomer and the cold leg. Approximately 45 sec after the initiation of HPI, we see a quenching behavior near the bottom of the cold leg (see readings of thermocouples L48 and L49). Because of penetration of the cold fluid, the fluid temperature drops about 5°C within 10 sec.

Figure 9 is the transient temperature plot for thermocouples at the core barrel side of the downcomer. The cold fluid leaving the cold leg directly hits the wall of the downcomer, as illustrated by the transient temperature plot of C_8 and C_9 in Fig. 9. Because Thermocouples C_{10} and C_{14} are located at the downcomer, well below the exit plane of the cold leg, the quenching behavior is not as pronounced as at locations of C_8 and C_9.

The transient temperature plots for thermocouples located at the pressure vessel side of the downcomer are presented in Fig. 10. The small disagreement between the computation and experiment may be attributed to the following:

- Non-isothermal conditions in the experiment at time t=0: Prior to the initiation of the HPI, the temperature was assumed to be uniform throughout--70°C. However, in the experiment, the initial temperatures for most of the thermocouples were well below 70°C.

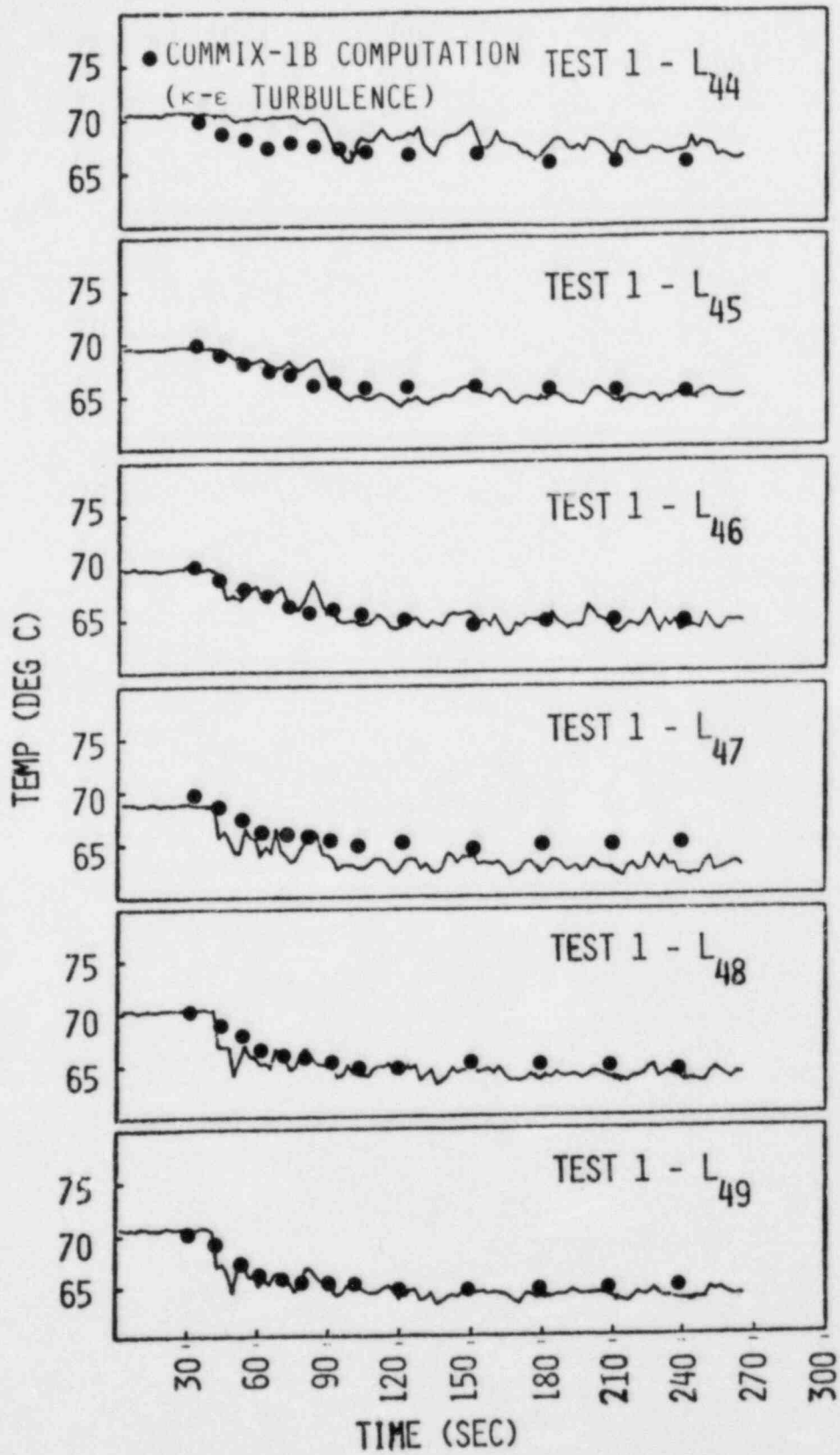

Fig. 8. Vertical Centerline Profile of Transient Temperatures in Cold Leg at Entrance to Downcomer - Test 1.

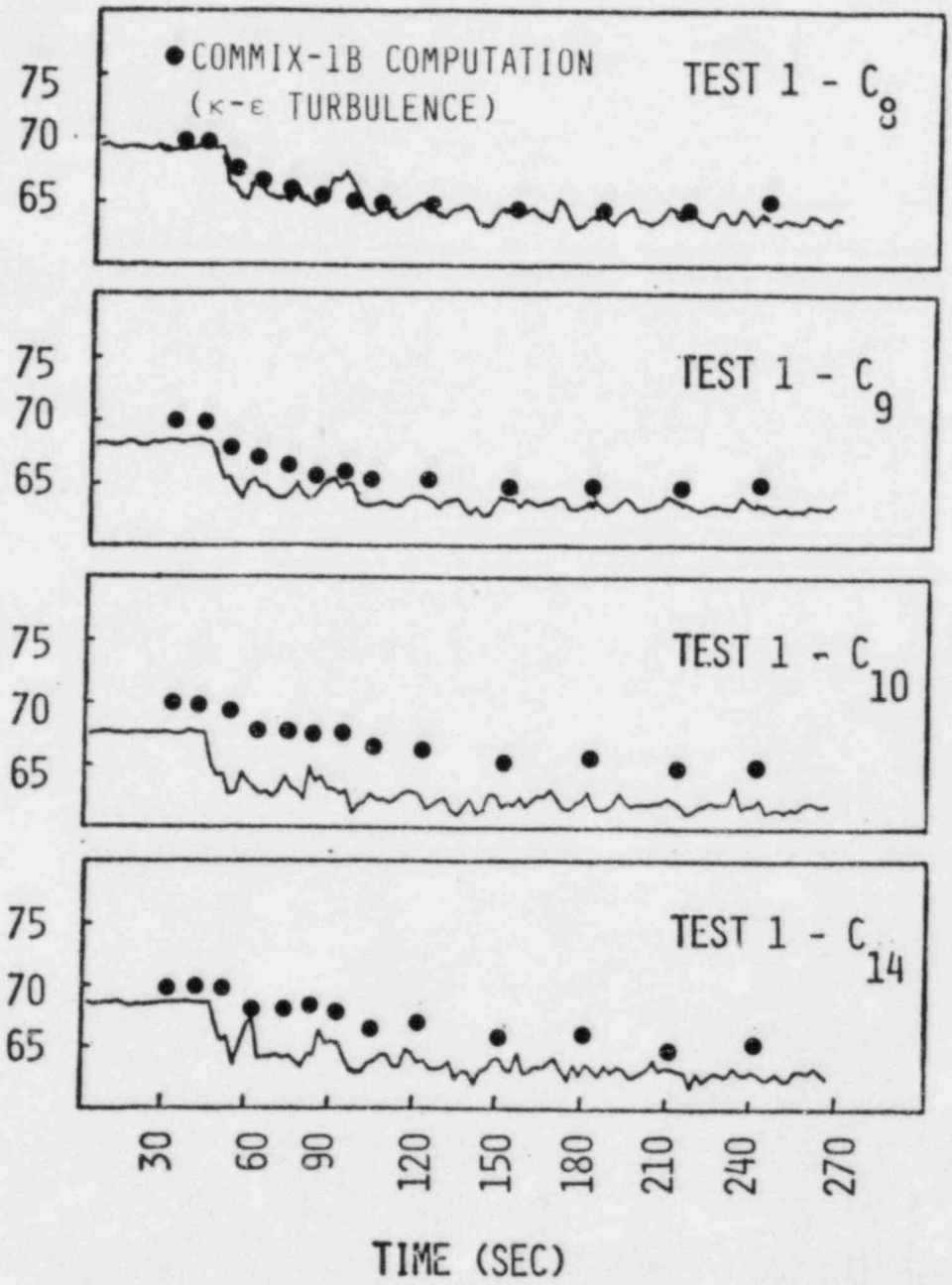

Fig. 9 Vertical Centerline Profile of Transient Temperature at Core-Barrel Side of Downcomer - Test 1

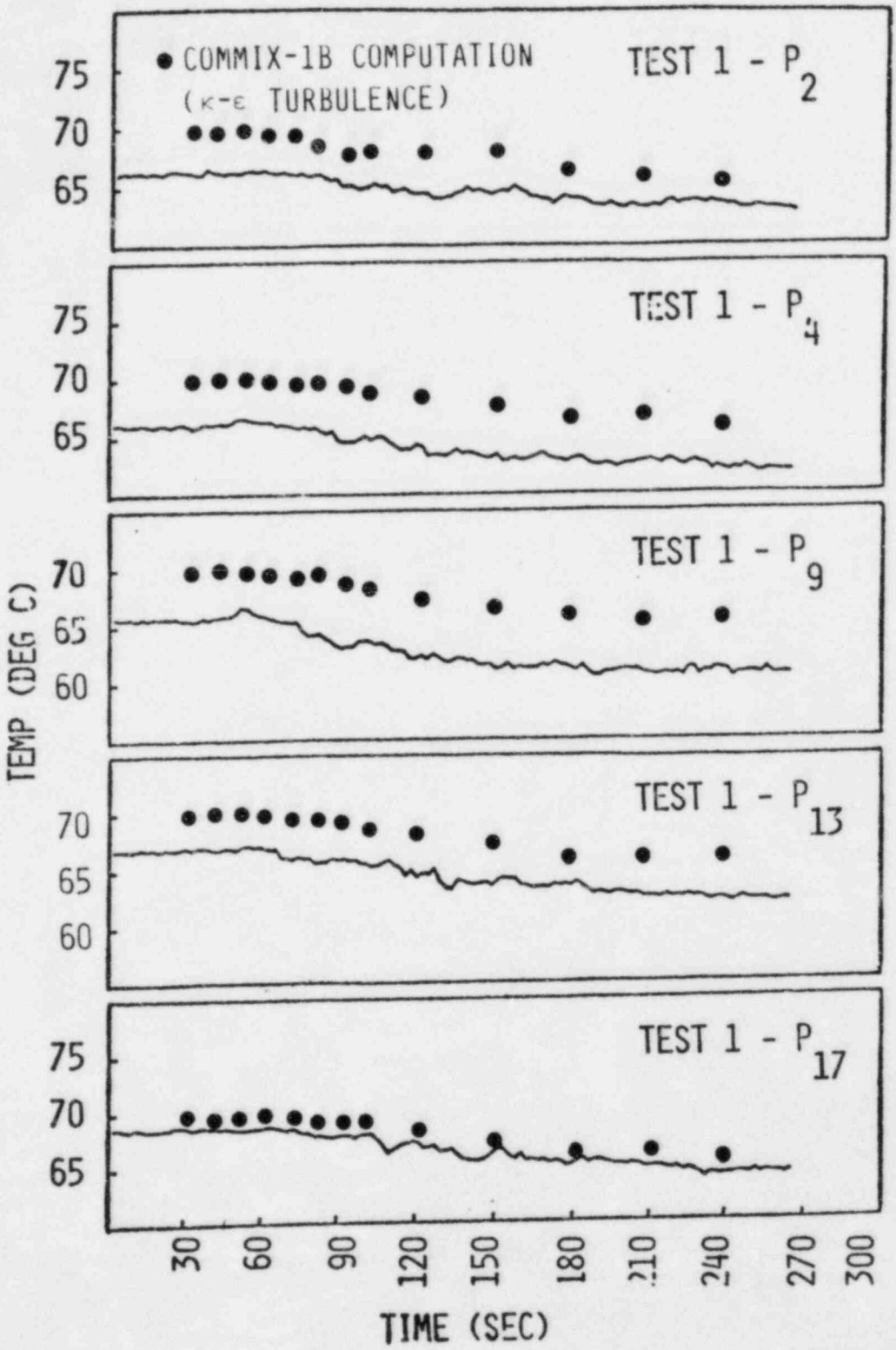

Fig. 10 Vertical Centerline Profile of Transient Temperature at Pressure-Vessel Side of Downcomer - Test 1

For example, at t=0 sec., the temperatures for P_2, P_4, and P_9 were only 67°C.

- Heat losses to the surrounding during experimentation: If heat losses to the surrounding area from the walls of the test section had been small, such as for Thermocouple P_{17}, the agreement would have been better.

7.3.4 Velocity Field

The vector plot of velocity profile at the central plane (y=0) at t = 254 seconds after the initiation of HPI, is shown in Fig. 11. At this time, the downcomer temperature is very close to the mixed mean temperature, indicating that an equilibrium has been established. Unfortunately, experimental data are not available for comparison.

The important mixing patterns to note are:

- Near the injector of the HPI, the cold fluid (17°C) from the HPI mixes with the hot fluid (70°C) in the cold leg.
- As the mixed fluid flows down the cold leg, the cold fluid from the top of the cold leg tends to penetrate to the bottom.
- At the junction of the cold leg and downcomer, the cold fluid is at the bottom; hot stagnant fluid from the downcomer tends to enter the cold leg at the top.
- In the downcomer, cold fluid impinges directly on the core barrel side of the downcomer like a wall jet.
- In the downcomer, after hitting the wall, cold fluid moves down along the core-barrel side until the downward motion is overcome by the upward momentum of the buoyancy-driven hot fluid. This creates a recirculating flow in the bottom section of the downcomer. As a result, the temperature gradient at the pressure-vessel side of the downcomer is relatively moderate.

To illustrate the effects of buoyancy forces in the cold leg and downcomer, the corresponding vector plot, but prior to the initiation of HPI, is shown in Fig. 12. Because the temperature is uniform, there are no buoyancy forces. As the buoyancy forces do not exist, we do not see any strong recirculating zones in Fig. 12 as we observed in the transient result (Fig. 11). The recirculating zone in the injector, prior to the initiation of HPI, is in the form of cavity flow.

7.3.5 Isotherms

The isotherm plot for y=0 plane at t = 254 sec is shown in Fig. 13. The temperature difference between two successive isotherms is 2°C. The temperature gradient is very large at the HPI location. We see a stable stratification as the cold leg fluid approaches the downcomer. The mixing in the lower part of the downcomer is quite good.

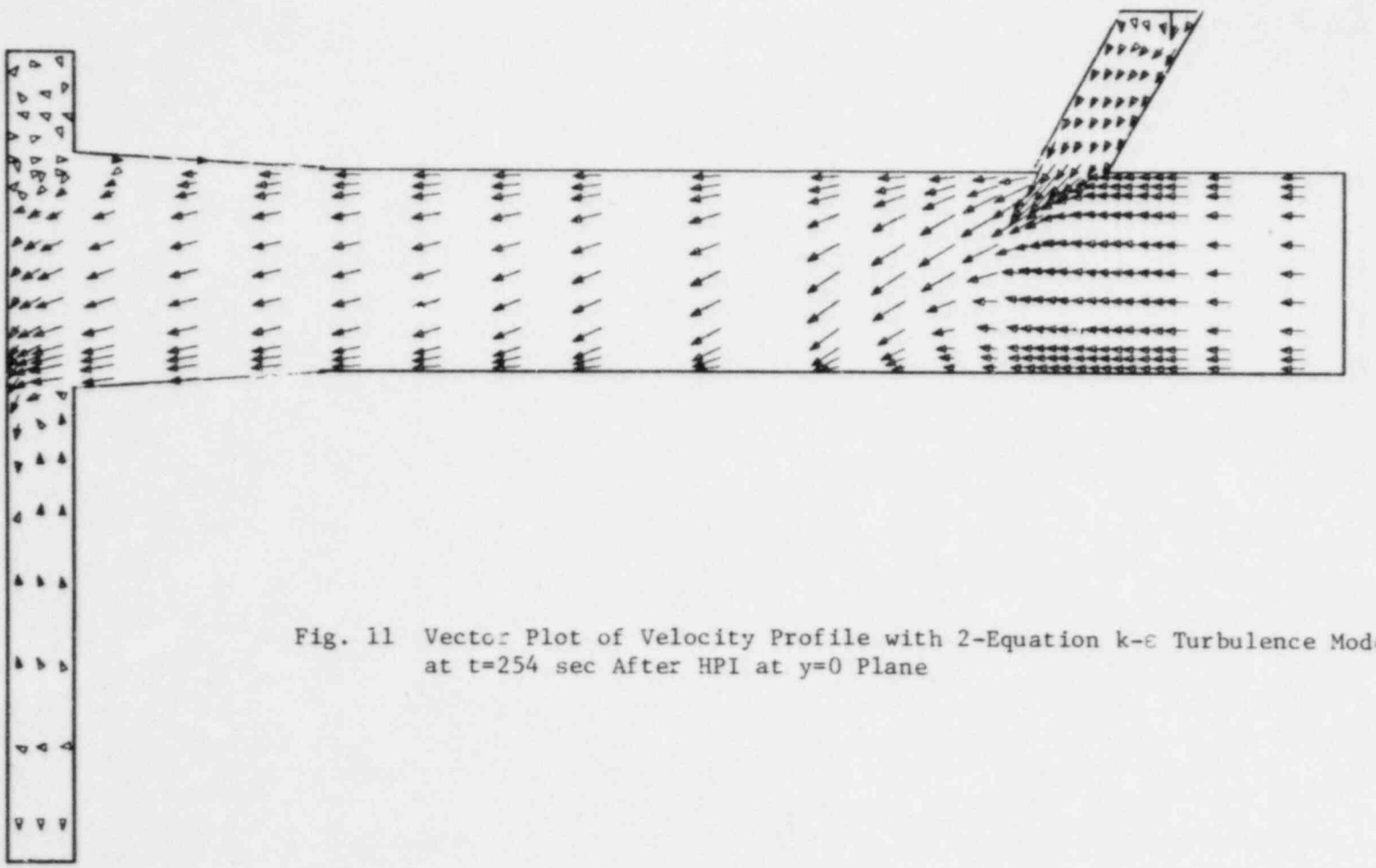

Fig. 11 Vector Plot of Velocity Profile with 2-Equation k-ε Turbulence Model at t=254 sec After HPI at y=0 Plane

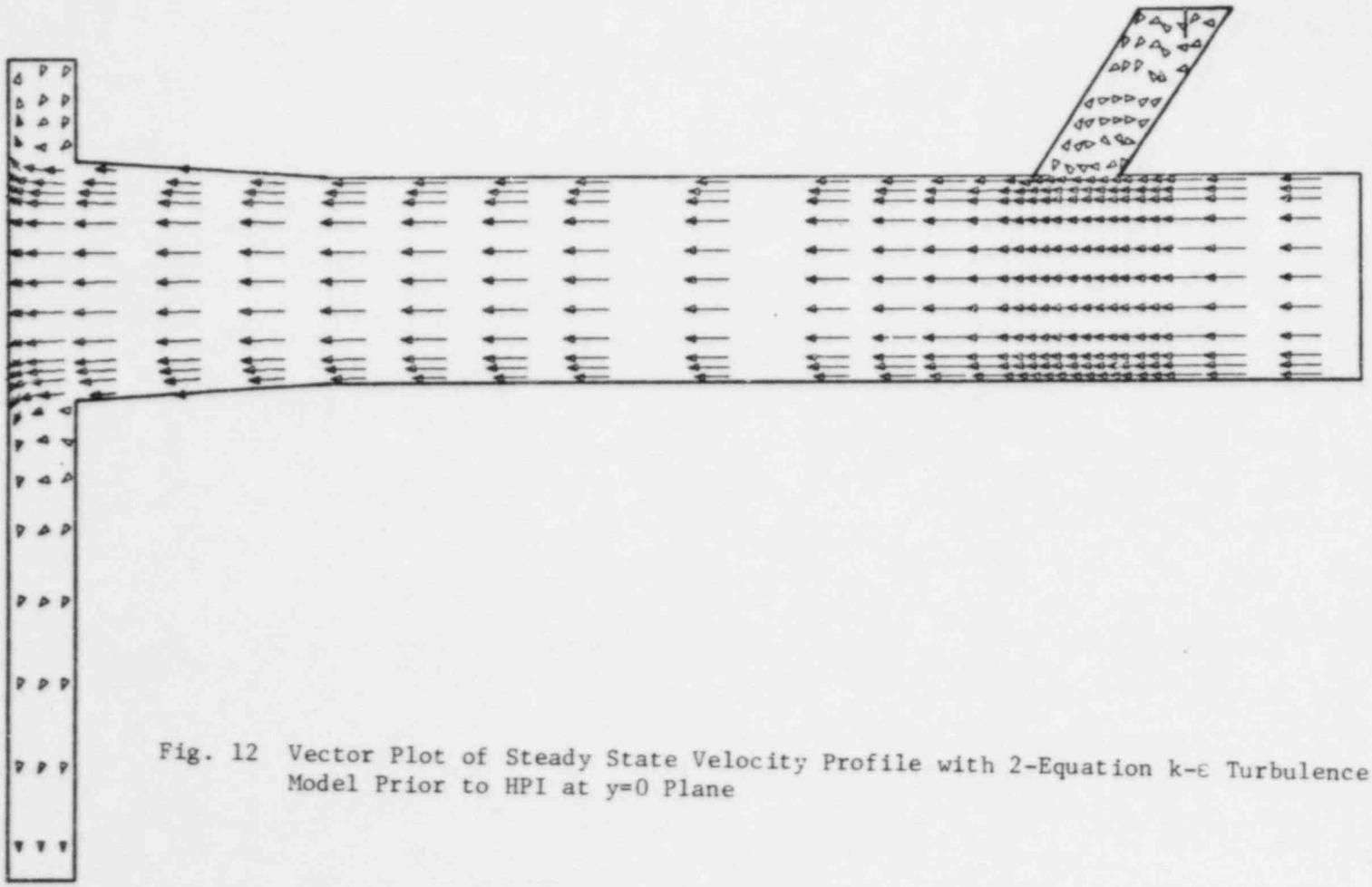

Fig. 12 Vector Plot of Steady State Velocity Profile with 2-Equation k-ε Turbulence Model Prior to HPI at y=0 Plane

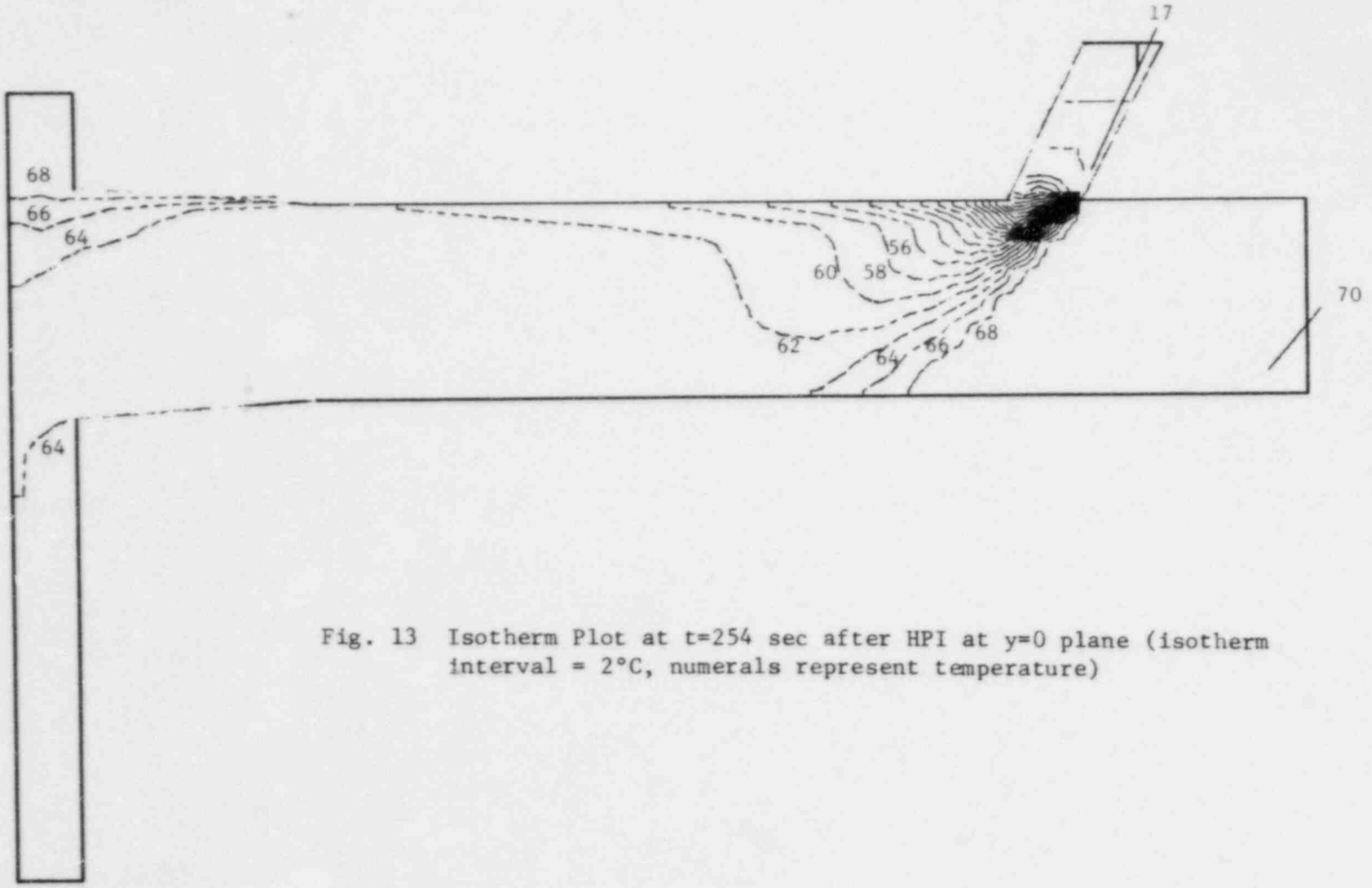

Fig. 13 Isotherm Plot at t=254 sec after HPI at y=0 plane (isotherm interval = 2°C, numerals represent temperature)

The isotherm plots for the core-barrel side and pressure side of the downcomer are shown in Figs. 14 and 15, respectively. The temperature difference between two successive isotherms is 1°C. In Fig. 14, at the core-barrel side of the downcomer, we see a relatively large cold zone. This, as mentioned before, is due to the impingement of the cold fluid from the cold leg and subsequent downward flow motion of this fluid. At the top portion of the downcomer, fluid motion is almost stagnant. Near the outlet of the downcomer, the fluid is well mixed. In Fig. 15, the corresponding cold zone at the pressure-vessel side is much smaller than that at the core-barrel side because of the upward motion of the buoyancy-driven fluid along the pressure-vessel side of the downcomer.

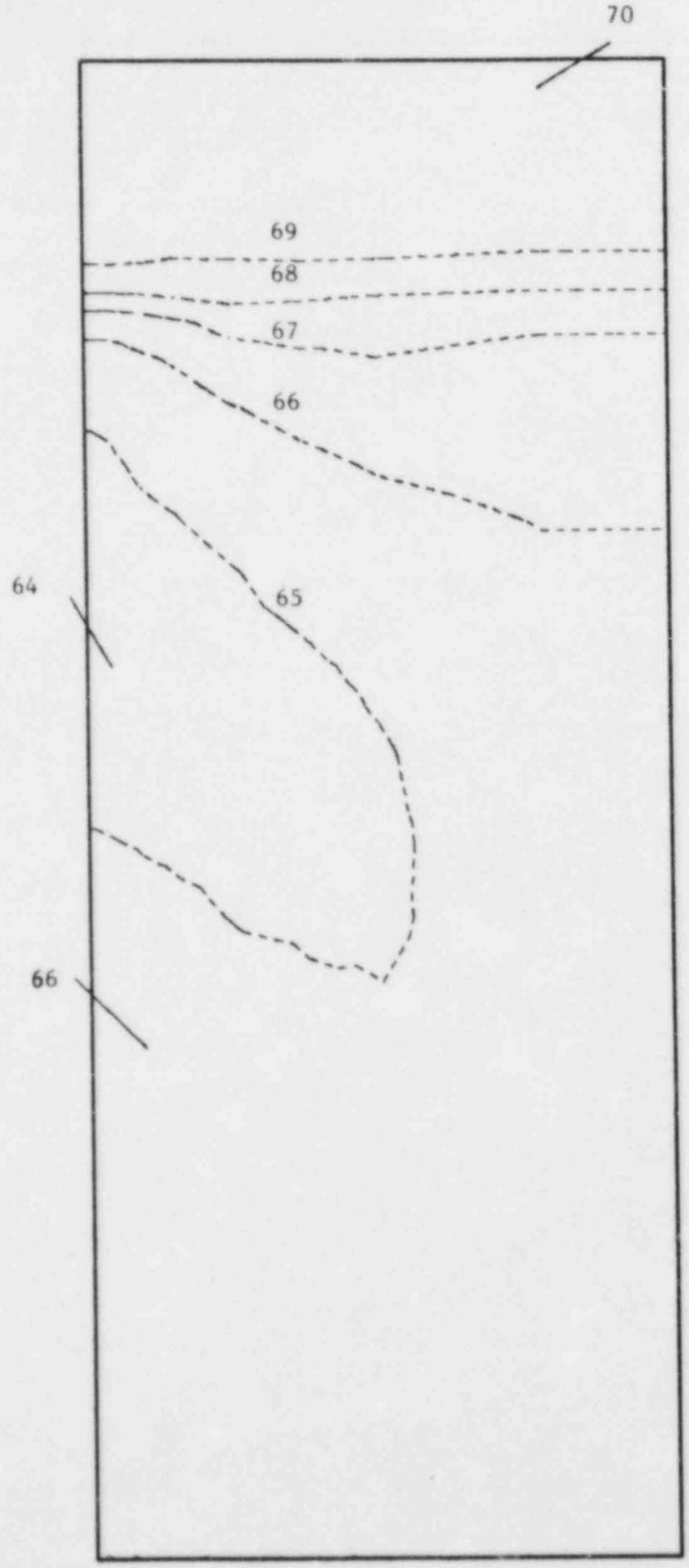

Fig. 14 Isotherm Plot at t=254 sec after HPI at Core-Barrel Side of Downcomer (isotherm interval = 1°C)

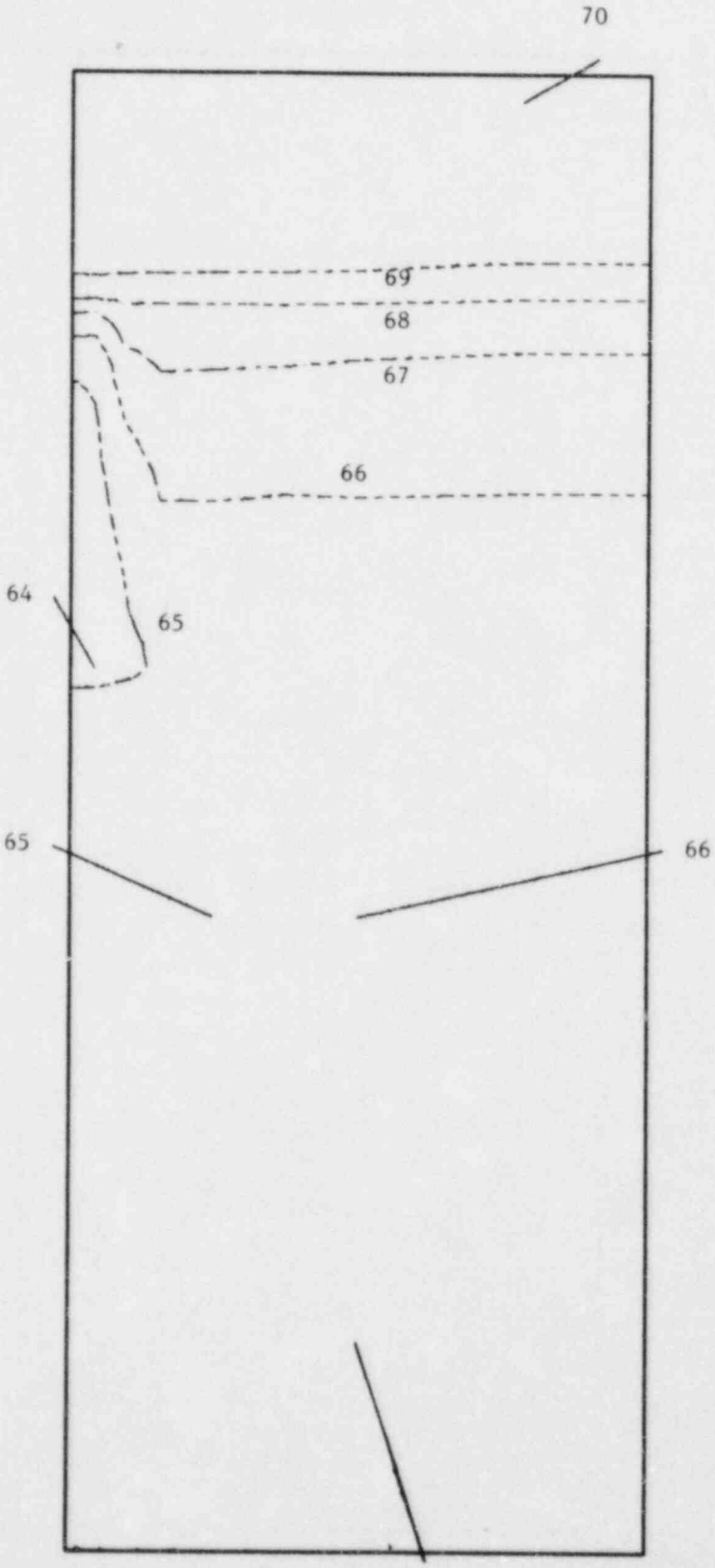

Fig. 15 Isotherm Plot at t=254 sec after HPI at Pressure Vessel Side of Downcomer (isotherm interval = 1°C)

8. CONCLUDING REMARKS

- Besides the simple constant turbulent viscosity model, three additional turbulence models (0-equation mixing-length, 1-equation (k) and 2-equation (k-ε) models) have been incorporated in the COMMIX code, thus, extending the range of applicability of COMMIX.

- These turbulent models are provided as options, and the user may select the one that is most appropriate for his or her application.

- For the three problems we have described, the 2-equation (k-ε) model predicts results that are best in agreement with experimental data.

- For flow having a dominant direction and without recirculation, the 0- equation mixing length and 1-equation (k) models are generally adequate. However, for recirculating and buoyancy driven flows, the 2-equation (k-ε) model generally gives better predictions than the 0- equation mixing length and 1-equation-k models.

- In the third problem, thermal and fluid mixing in the cold leg and downcomer of a PWR, we have performed two simulations with the 2-equation (k-ε) model. Although the results of both simulations are in reasonable agreement with experimental data, the calculation with the 2-equation (k-ε) turbulence model and VWSUD scheme agrees better with the experimental results

- All of the simulations, except Case 4 of the third problem, were performed with the the pure-upwind difference scheme, which might have caused some numerical diffusion. A new Volume-Weighted Skew-Upwind Difference scheme has been implemented that substantially decreases the amount of numerical diffusion. A report describing the VWSUD scheme has been prepared[24].

- There is no universal turbulence model; furthermore, a turbulence model is highly geometry-dependent. In addition, the results may also depend on the values of k and ε prescribed at the inlet planes. Therefore, to further validate the turbulence models implemented in COMMIX-1B, more analyses in the pressurized thermal shock and other applications are needed.

ACKNOWLEDGEMENTS

We are indebted to all our colleagues in the Analytical Thermal Hydraulic Research Program and especially Drs. C. I. Yang and S. P. Vanka for their stimulating discussions and contributions, and to Professors B. T. Chao and S. L. Soo for their constructive comments; to Mrs. S. A. Moll and Miss B. D. Wright for typing the manuscript; to Drs. R. T. Curtis, and C. N. Kelber and Mr. P. M. Wood of the U. S. Nuclear Regulatory Commission for their support in the development work; and to Drs. J. H. Kim, B. K. H. Sun, and W. B. Loewenstein for their support in the validation work.

REFERENCES

1. W. T. Sha and B. T. Chao, "Local Volume-Averaged Transport Equations for Single-Phase Flow in Regions Containing Fixed, Dispersed Heat-Generating (or Absorbing) Solids," NUREG/CR-1969, ANL-80-124 (Apr. 1981).

2. W. T. Sha, B. T. Chao, and S. L. Soo, "Local Volume-Averaged Transport Equations for Multiphase Flow in Regions Containing Distributed Solid Structures," NUREG/CR-2354, ANL-81-69 (Dec. 1981).

3. W. T. Sha, H. M. Domanus, R. C. Schmitt, J. J. Oras, and E. I. H. Lin, "COMMIX-1: A Three-Dimensional, Transient, Single-Phase Component Computer Program for Thermal-Hydraulic Analysis," NUREG/CR-0415, ANL-77-96 (DRAFT) (Jan. 1978).

4. H. M. Domanus, W. T. Sha, R. C. Schmitt, and V. L. Sha, "COMMIX-1A: A Three-Dimensional Transient Single-Phase Computer Program for Thermal Hydraulic Analysis of Single and Multicomponent Systems," NUREG/CR-2896, ANL-82-25 (to be published in 1983).

5. L. Prandtl, "Bericht uber Untersuchungen zer ansgebil-derter Turbulenz," ZAMM, Vol. 5, pp. 136-139 (1925).

6. L. Prandtl, Nach. Akad. Wiss. Goett. Math-Phys. Kl. (1945); translated as Jet Propul. Lab. Publication 13 (1952).

7. P. Bradshaw, D. H. Ferris, and N. P. Atwell, "Calculation of Boundary Layer Development Using the Turbulent Energy Equation," J. Fluid Mech., Vol. 28, p. 593 (19 ').

8. V. W. Nee and L. S. G. Kovasznay, "The Calculation of the Incompressible Turbulent Boundary Layer by a Simple Theory," Physics of Fluids, Vol. 12, p. 473 (1969).

9. F. H. Harlow and P. I. Nakayama, "Transport of Turbulence Energy Decay," Los Alamos Scientific Lab. Report LA-3854/UC-34 physics/TID-4500 (1968).

10. W. P. Jones and B. E. Launder, "The Prediction of Laminarization with a 2-equation Model of Turbulence," Int. J. Heat Mass Trans., Vol. 15, pp. 301-313 (1982).

11. P. Y. Chou, "On Velocity Correlation and Solution of the Equations of Turbulenct Fluctuations, "Q. J. Mech. Appl. Math., Vol. 3, pp. 38-54 (1945).

12. K. Hanjalic and B. E. Launder, "A Reynolds-Stress Model of Turbulence and its Application to Asymmetric Shear Flows," J. Fluid Mech., Vol. 52, pp. 609-638 (1972).

13. B. E. Launder, G. J. Reese, and W. Rodi, "Progress in the Development of a Reynolds-Stress Turbulent Closure," J. Fluid Mech., Vol. 68, pp. 537-566 (1975).

14. W. T. Sha and B. E. Launder, personal communication (1979).

15. H. Tenneke and J. L. Lumley, "A First Course in Turbulence, MIT Press, Cambridge, MA (1972).

16. B. J. Daly and F. H. Harlow, "Transport Equations in Turbulence," Physics of Fluids, Vol. 13, pp. 2634-2649 (1970).

17. J. L. Lumley and B. J. Khajeh-Nouri, "Computational Modeling of Turbulent Transport," Adv. Geophysics, Vol. 18A, pp. 169-192 (1974).

18. W. P. Jones and B. E. Launder, "The Calculation of Low-Reynolds-Number Phenomena with a Two-Equation Model of Turbulence," Int. J. Heat. Mass Trans., Vol. 16, pp. 1119-1130 (1973).

19. B. E. Launder, A. Morse, W. Rodi, and D. B. Spalding, "The Prediction of Free Shear Flows - A Comparison of the Performance of Six Turbulent Models," Proc. of NASA Conference on Free Shear Flows, Langbery (1972).

20. A. R. Barbin and J. B. Jones, "Turbulent Flow in the Inlet Region of a Smooth Pipe," J. Basic Engineering, Trans. ASME, Vol. 85, p. 29 (1963).

21. M. C. Chaturvedi, "Flow Characteristics of Axisymetric Expansion," J. Hydraulics Division, Proc. of ASCE, p. 1 (1963).

22. A. Hashemi and J. Goodman, "Thermal Mixing in a Rectangular Geometry Model of a Cold Leg with High Pressure Injection and a Downcomer," Science Applications Inc., EPRI NP-2924 (Mar. 1983).

23. C. L. Lin, J. H. Kim, and B. K. H. Sun, "Numerical Simulation of Thermal and Fluid Mixing in the Cold Leg and Downcomer of a Model Geometry during a PWR Primary Side Overcooling," Thermal-Hydraulics of Nuclear Reactors, Vol. II, The Second International Topical Meeting on Nuclear Reactor Thermal-Hydraulics, Santa Barbara, CA U.S.A, pp. 988-996 (Jan 11-14, 1983).

24. C. C. Miao, R. W. Lyczkowski, G. K. Leaf, F. F. Chen, B. C. Cha, B. C-J. Chen, H. M. Domanus, W. T. Sha, and V. L. Shah, "A Volume-Weighted Skew-Upwind Difference Scheme in COMMIX," NUREG/CR-3505, EPRI NP-3547, ANL-83-66 (Mar. 1984).

25. R. W. Lyczkowski, C. C. Miao, H. M. Domanus, J. R. Hull, W. T. Sha, and R. C. Schmitt, "Three-Dimensional Analysis of Thermal and Fluid Mixing in Cold Leg and the Downcomer of PWR Geometries," EPRI NP-3321 (Dec. 1983).

Distribution for NUREG/CR-3504, EPRI NP-3546, ANL-83-65

Internal:

E. S. Beckjord
C. E. Till
R. S. Zeno
P. B. Abramson
M. L. Bottoni
A. R. Brunsvold
B. K. Cha
Y. S. Cha
B. C-J. Chen
F. F. Chen
W. L. Chen
H-N. Chi
T. Chiang
T. H. Chien
D. H. Cho
L. W. Deitrich
H. M. Domanus
D. R. Ferguson
P. L. Garner
J. R. Hull
M. Ishii
J. F. Kuzanek
G. K. Leaf
R. W. Lyczkowski
D. Malloy
C. C. Miao
R. C. Schmitt
W. T. Sha (45)
V. L. Shah (45)
Y. W. Shin
R. M. Singer
J. E. Sullivan
D. P. Weber
C. I. Yang
S. K. Zussman
ANL Patent Dept.
ANL Contract File
ANL Libraries (2)
TIS Files (3)

External:

USNRC, Washington, for distribution per R7 (250)
DOE-TIC (2)
Manager, Chicago Operations Office, DOE-CH
Components Technology Division Review Commmittee:
D. J. Anthony, General Electric Co., Schenectady, NY 12345
A. A. Bishop, U. Pittsburgh, Pittsburgh, PA 15261
B. A. Boley, Northwestern University, Evanston, IL 60201
F. W. Buckman, Wood-Leaver and Associates, Monroeville, PA 15146
R. Cohen, Purdue U., West Lafayette, IN 47907
J. Weisman, U. Cincinnati, Cincinnati, OH 35221
B. T. Chao, U. Illinois, Urbana, IL 61801
E. L. Gluekler, General Electric Co., Sunnyvale, CA 94086
M. S. Kazimi, Masschusetts Institute of Technology, Cambridge, MA 02139
J. H. Kim, Electric Power Research Institute, Palo Alto, CA 94303 (3)
G. S. Lellouche, Electric Power Research Institute, Palo Alto, CA 94303
R. Markley, Westinghouse Advanced Reactors Division, Madison, PA 15663
J. C. Mills, Atomics International, Canoga Park, CA 91306
A. L. Schor, Massachusetts Institute of Technology, Cambridge, MA 03129
B. R. Sehgal, Electric Power Research Institute, Palo Alto, CA 94303
J. C. Slattery, Northwestern U., Evanston, IL 61801
S. L. Soo, U. Illinois, Urbana, IL 61801
J. R. Thompson, Mississippi State U., Mississippi State, MS 39762
N. E. Todreas, Massachusetts Institute of Technology, Cambridge, MA 02139
B. K. H. Sun, Electric Power Research Institute, Palo Alto, CA 94303
R. B. Duffey, Electric Power Research Institute, Palo Alto, CA 94303
A. Singh, Electric Power Research Institute, Palo Alto, CA 94303
J. P. Sursock, Electric Power Research Institute, Palo Alto, CA 94303
W. B. Loewenstein, Electric Power Research Institute, Palo Alto, CA 94303

NRC FORM 335 (11-81)

U.S. NUCLEAR REGULATORY COMMISSION

BIBLIOGRAPHIC DATA SHEET

1. REPORT NUMBER (Assigned by DDC)
NUREG/CR-3504
ANL-83-65, EPRI NP-3546

4. TITLE AND SUBTITLE (Add Volume No., if appropriate)
TURBULENCE MODELING IN THE COMMIX COMPUTER CODE

2. (Leave blank)

3. RECIPIENT'S ACCESSION NO.

7. AUTHOR(S)
F. F. Chen, H. M. Domanus, W. T. Sha, and V. L. Shah

5. DATE REPORT COMPLETED
MONTH: February YEAR: 1984

9. PERFORMING ORGANIZATION NAME AND MAILING ADDRESS (Include Zip Code)
Argonne National Laboratory
9700 South Cass Avenue
Argonne, Illinois 60439

DATE REPORT ISSUED
MONTH: May YEAR: 1984

6. (Leave blank)

8. (Leave blank)

12. SPONSORING ORGANIZATION NAME AND MAILING ADDRESS (Include Zip Code)
Containment Research Systems Branch
Division of Accident Evaluation
Office of Nuclear Regulatory Research
U.S. Nuclear Regulatory Commission
Washington, D.C. 20555

10. PROJECT/TASK/WORK UNIT NO.

11. FIN NO.
A2045

13. TYPE OF REPORT
Technical

PERIOD COVERED (Inclusive dates)
May 1982 - February 1984

15. SUPPLEMENTARY NOTES

14. (Leave blank)

16. ABSTRACT (200 words or less)

The report describes the three additional turbulence models [0-equation (mixing-length), 1-equation (k), and 2-equation (k-ε)] recently implemented in the COMMIX-1B computer code. COMMIX-1B is a three-dimensional, steady-state/transient, single-phase computer code for thermal-hydraulic analysis of single/multicomponent systems under normal and off-normal operating conditions. All three turbulence models are provided as options, and a user can select the one that is most appropriate for his or her application.

To validate these turbulence models, we have performed several numerical simulations and compared the results with experimental data. Three of the simulations--turbulent flow in a pipe, flow in a circular duct with sudden expansion, and thermal and fluid mixing in the cold leg and downcomer of a PWR--are presented here along with their comparisons with experimental data. More analyses are needed for further validation. Incorporation of the three turbulence models has expanded the range of application of the COMMIX code.

17. KEY WORDS AND DOCUMENT ANALYSIS

17a. DESCRIPTORS

Turbulence Models
Thermal Hydraulics
Numerical Analysis
Finite Difference Solutions

17b. IDENTIFIERS/OPEN-ENDED TERMS

18. AVAILABILITY STATEMENT
UNLIMITED

19. SECURITY CLASS (This report)
Unclassified

21. NO. OF PAGES
48

20. SECURITY CLASS (This page)
Unclassified

22. PRICE
$

NRC FORM 335 (11-81)